Registered Office
Herrmann-Debrouxlaan 40
1160 Brussel – Belgium

Foundation of Public Utility
VAT BE 406.568.867

Research Centres
Boeretang 200
2400 Mol – Belgium

Chemin du Cyclotron 6
1348 Ottignies-Louvain-la-Neuve – Belgium

Reference N°	Creation Date	
SCK CEN/44404374	2022-01-25	
Alternative Reference N°	Revision	Version
N/A	1.0	3
ISC	Revision Status	
Restricted	Approved	

Masterthesis-AlexanderVermunicht.docx

Authors*
Meryem Arman

Approval information for current revision*		
Name	**Outcome**	**Date**
Thomas Cardinaels	Approved	2022-01-26

Change log*				
Revision	**Version**	**Status**	**Date**	**Description of change**
1.0	3	Approved	2022-01-25	

**This automatically generated cover page shows references and document information as were available in the Alexandria document management system on 2022-01-26. Please refer to Alexandria for current and complete metadata, or to the document contents and/or author for additional information.*

KU LEUVEN

FACULTEIT WETENSCHAPPEN

Electrochemical Oxidation of Terbium(III) in Aqueous Carbonate Solutions

Alexander VERMUNICHT

Promotor: Prof. T. Cardinaels
KU Leuven / SCK CEN

Co-promotor: Prof. K. Binnemans
KU Leuven

Mentor: B. Geboes
SCK CEN

Mentor: M. Arman
KU Leuven / SCK CEN

Proefschrift ingediend tot het
Behalen van de graad van
Master of Science
in Chemie

Academiejaar 2020-2021

SCK CEN/44404374 Rev. 1.0

Acknowledgements/Preface

To obtain my master's degree I have written my master's thesis, however this would not have been possible without the help and support of several people. Therefore I want to take this opportunity to thank those who assisted me the past year.

First of all I want to start by thanking my mentors, Meryem Arman with whom I've been in contact on an almost daily basis and Bart Geboes with whom I discussed my obtained results every week. In the weekly meetings they adjusted the plan of approach in consultation with me, when necessary. I want to thank them especially because of their friendly and approachable attitude, which motivated me to finish the best possible version of my thesis.

I want to thank my promotor and co-promotor, professor Cardinaels and professor Binnemans for making this project possible, in which I was allowed to participate. Despite the nerves I sometimes felt during presentations, the meetings were always very enlightening.

I would also like to express my thanks towards the other employees and students at SCK CEN. In particular for the positive atmosphere in the lab and the willingness to help me find my way around the lab.

Last but not least I would like to thank my family and friends for the mental support they gave me during this thesis. It definitely was not an easy task, as due to COVID-19 restrictions, social gatherings were limited the past year.

Summary

Radiopharmaceuticals are widely implemented in the therapy and diagnosis of cancers. Since such radiotherapy is a relatively new method it's still researched intensively to further improve the currently used techniques. ^{177}Lu is a radionuclide used for cancer therapy with its decay of β^- particles accompanied by photons suitable for SPECT imaging. A possibly improved alternative was found for ^{177}Lu, namely ^{161}Tb. The decay properties of ^{161}Tb are very similar compared to those of ^{177}Lu, however the main advantage is the amount of Auger electrons emitted per decay, ^{161}Tb emits 16x more Auger electrons per decay. These Auger electrons are a desired type of emitted particles as they have a high linear energy transfer (LET), being able to damage unwanted tissue at a short range. ^{161}Tb can be produced by neutron capture of ^{160}Gd in a nuclear reactor. The difficulty of ^{161}Tb production lies in the purification from the stable target material ^{160}Gd. The separation of different lanthanides can be facilitated by selectively changing the oxidation state of the one to be extracted. The selective electrochemical oxidation of Tb^{3+} in aqueous carbonate solutions is investigated in this thesis.

The quantification of produced Tb^{4+} by the measured current response at the working electrode during oxidation was not possible, because the measured current was caused by both the oxidation of Tb^{3+} and the oxidation of water to oxygen gas. For this reason the electrochemical reduction of Tb^{4+} was investigated with the goal of indirectly quantifying Tb^{4+} by reducing it back to Tb^{3+}.

Several parameters were varied to determine the influence on the electrochemical oxidation of Tb^{3+} in aqueous carbonate solutions. The concentrations of Tb and K_2CO_3 were investigated and optimized. The influence of pH was found to be crucial regarding the stability of Tb^{4+} complex. Furthermore kinetics was researched by varying the temperature.

In addition to these, two types of flow cells were used for the electrochemical oxidation of Tb^{3+} to see the impact of electrode surface ratio on the system. To test the influence of the flow on a general electrolytic system, exploratory experiments were run using a dilute sulfuric acid in combination with a Pt working electrode.

Finally, as a second type of cell which differs from the standard bulk electrolysis cell, a divided cell was tested. The counter electrode was separated from the rest of the cell using a semi-permeable membrane, preventing possible back reduction and therefore improving the efficiency. The two types of membranes tested were a CoralPor® frit and a more standard porous glass frit. For both membranes the resistance resulting from the separation was determined.

Samenvatting

Radiofarmaceutica worden vandaag de dag reeds op grote schaal toegepast, zowel voor de therapie als diagnose van kankercellen. Aangezien bestralingstherapie een relatief nieuwe behandelingsmethode is, wordt er nog steeds intensief onderzoek verricht om de momenteel gebruikte technieken verder te optimaliseren. ^{177}Lu is een radionuclide die momenteel gebruikt wordt voor kankertherapie, waarbij het verval van β^--deeltjes gepaard gaat met fotonen die geschikt zijn voor SPECT-beeldvorming. Een mogelijks beter alternatief voor ^{177}Lu werd gevonden, namelijk ^{161}Tb. De vervaleigenschappen van ^{161}Tb zijn zeer gelijkaardig aan die van ^{177}Lu, maar het belangrijkste voordeel zit hem in het aantal Auger-elektronen die per verval worden uitgezonden: ^{161}Tb zendt 16x meer Auger-elektronen uit per verval. Deze Auger-elektronen zijn zeer gewenst aangezien zij een hoge lineaire energieoverdracht hebben, waardoor ze op korte afstand schade kunnen toebrengen aan kwaadaardig weefsel. ^{161}Tb wordt geproduceerd door het bestralen van ^{160}Gd met neutronen in een kernreactor. De moeilijkheid bij de productie van ^{161}Tb bevindt zich in het opzuiveren uit het stabiele basismateriaal ^{160}Gd. De scheiding van verschillende, gelijkaardig lanthaniden kan worden vergemakkelijkt door de oxidatietoestand van het te extraheren product selectief te wijzigen. De selectieve elektrochemische oxidatie van Tb^{3+} in waterige carbonaatoplossingen wordt in dit proefschrift onderzocht.

De kwantificering van geproduceerd Tb^{4+} op basis van de gemeten stroomrespons aan de werkelektrode tijdens de oxidatie was niet mogelijk, omdat de gemeten stroom zowel door de oxidatie van Tb^{3+} als door de oxidatie van water tot zuurstofgas werd veroorzaakt. Om deze reden werd de elektrochemische reductie van Tb^{4+} onderzocht met als doel Tb^{4+} indirect te kwantificeren door het terug te reduceren tot Tb^{3+}.

Verschillende parameters werden gevarieerd om hun invloed op de elektrochemische oxidatie van Tb^{3+} in waterige carbonaatoplossing te bepalen. De concentraties van terbium en K_2CO_3 werden onderzocht en geoptimaliseerd. Tenslotte werd de kinetica onderzocht door het variëren van de temperatuur van de oplossing.

Daarnaast werden twee soorten doorstroomcellen gebruikt voor de elektrochemische oxidatie van Tb^{3+} om de invloed van de verhouding van het elektrodeoppervlak op het systeem te bekijken. Om de invloed van het debiet op een algemeen elektrolytisch systeem te testen, werden verkennende experimenten uitgevoerd met een verdund zwavelzuur in combinatie met een Pt-werkelektrode.

Tenslotte werd, als tweede celtype dat afwijkt van de standaard bulk elektrolysecel, een gesplitste cel getest. De tegenelektrode werd van de rest van de cel gescheiden met behulp

van een semipermeabel membraan, waardoor mogelijke terugreductie werd voorkomen en derhalve het rendement werd verbeterd. De twee geteste membraantypes waren een CoralPor® frit en een meer standaard poreuze glasfrit. Voor beide membranen werd de weerstand als gevolg van de scheiding van de elektroden bepaald.

List of abbreviations

SPECT	single photon emission computed tomography
PET	positron emission tomography
LET	linear energy transfer
$t_{1/2}$	half-life
IAEA	International Atomic Energy Agency
BR2	Belgian Reactor 2
EDTA	ethylenediaminetetraacetic acid
HEH[EHP]	2-ethylhexylphosphonic acid mono-2-ethylhexyl ester
HDEHP	di-(2-ethylhexyl)phosphoric acid
E%	extraction yield
D	distribution ratio
SHE	standard hydrogen electrode
GC	glassy carbon
CGE	conducting glass electrode
TPPO	triphenylphosphine oxide
TPAsO	triphenyl arsine oxide
ε	molar absorptivity
WE	working electrode
CE	counter electrode
RE	reference electrode
RVC	reticulated vitreous carbon
EIS	electronic impedance spectroscopy
CV	cyclic voltammetry
LMCT	ligand to metal charge transfer
LSV	linear sweep voltammetry
ORR	oxygen reduction reaction

List of Figures and Tables

Table of contents

I. Introduction

1. Medical radiolanthanides

1.1. Nuclear medicine and the share of radiolanthanides

Cancer is one of the most researched diseases worldwide, mainly because it is a disease which occurs in all groups of society and there is no treatment that fits for all. There are several types of treatment paths, including chemotherapy, radiative nuclear therapy and immunotherapy. Radiative therapy is used in 40% of all cancer treatments worldwide, because of its quality of specifically targeting tumor cells while minimizing the damage to healthy cells.[1] It is often implemented as part of a combined treatment method.[2]

Radiopharmaceuticals consist of radionuclides that decay in a specific way and of biomolecules with targeting properties. These drugs can be used as a diagnostic drug by noninvasive imaging or as a therapeutic drug where toxic radiation is delivered to targeted tissue. The difference between diagnostic and therapeutic radionuclides is found in the decay mode, which on its turn correlates to the decay energy. Diagnostic agents decay via photon emission with high enough energy to penetrate through the body and to be detected outside the body. Whereas therapeutic agents decay via emission of a particle like α or β^-, causing ionization to nearby tissue.[3]

There are 2 main diagnostic techniques that differ from each other by the emitted particle and with it the detection technique; SPECT (single photon emission computed tomography) is based on radionuclides emitting photons with an energy between 70 and 360 keV.[3] PET (positron emission tomography) is an imaging technique based on radionuclides which mainly decay via positron emission. On its turn the positron annihilates with an electron, producing two photons of 511 keV each in opposite directions. SPECT is the most commonly used noninvasive imaging technique because PET radionuclides have the disadvantage of having a very short half-life making it more difficult to integrate the isotopes in biomolecules. PET is also the more expensive technique.[4]

The field of diagnostic imaging is mainly dominated by technetium-99m.[3,5] This radionuclide is so popular because of its ideal radiative properties: emission of a single photon at 140 keV, no simultaneous particle emission, an optimal half-life of 6.03 hours and it is easy accessible from portable isotope generators. However, when looking at therapeutic drugs a variety of radionuclides is used. Different types and properties of decays are necessary to provide a variety in medical techniques required for different treatments of cancerous tissue. When selecting a therapeutic radionuclide, several factors must be considered to optimize the damage done to the tumor tissue and to minimize damage done to healthy tissue.

For various types and sizes of tumors different half-life ($t_{1/2}$), energy of emitted particles and specific activity are required. Emitted ionizing particles can be α, β^- or Auger electrons.[3] The low energy β^- emitter is more optimal for smaller target tissues, whereas the higher energy β^- is better for larger target tissues. Also availability and cost of the radionuclide play a role in the decision of what isotope to use. The most used therapeutic radionuclides are iodine-131, yttrium-90 and rhenium-186.[3]

The group of lanthanides and lanthanide-like elements (scandium and yttrium) are getting more interest over the last couple of years because of their interesting properties. Due to their varying nuclear properties they allow a variety of decay properties such as decay types, energies and half-lives. Because of their similar chemical properties and their main occurrence as M^{3+} in aqueous solution, they show similar production routes for radiopharmaceuticals, using similar biomolecules.[3,5–7]

Table 1: Characteristics of most important reactor produced β^- emitting radiolanthanides with accompanying γ emission studied for radionuclide therapy. For the ^{164}Dy(2n,γ) reaction, the thermal neutron cross section of ^{165}Dy intermediate is given. Also the lanthanide-like isotopes ^{47}Sc and ^{90}Y are included. Table copied from Van de Voorde et al.[8]

Radionuclide	Half-life	Major production route [a]	σ_{th} (barn)	$E_{\beta,max}$ (keV)	$E_{\gamma,main}$ (keV) (% ab)
^{143}Pr	13.6 d	^{142}Ce(n,γ)^{143}Ce → β^-	0.95	933	742 (38.5)
^{149}Pm	2.21 d	^{148}Nd(n,γ)^{149}Nd → β^-	2.503	1 071	285 (2.8)
^{153}Sm	1.95 d	^{152}Sm(n,γ)	206.2	808	103.2 (28.3)
^{161}Tb	6.91 d	^{160}Gd(n,γ)^{161}Gd → β^-	1.5	593	74.6 (5.8)
^{165}Dy	2.33 h	^{164}Dy(n,γ)	2720	1 286	94.7 (3.6)
^{166}Ho	1.12 d	^{165}Ho(n,γ)	61.2	1854	80.6 (6.2)
		^{164}Dy(2n,γ)^{166}Dy → β^-	3900		
^{169}Er	9.40 d	^{168}Er(n,γ)	1.28	350	84 (0.16)
^{170}Tm	128.4 d	^{169}Tm(n,γ)	109	968	84 (3.26)
^{177}Lu	6.65 d	^{176}Yb(n,γ)^{177}Yb → β^-	2.85	498	208.4 (11.1)
		^{176}Lu(n,γ)	2090		
^{47}Sc	3.35 d	^{46}Ca(n,γ)^{47}Ca → β^-	0.7405	600	159.4 (68)
		^{47}Ti(n,p)^{47}Sc			
^{90}Y	2.67 d	^{89}Y(n,γ)^{90}Y	1.287	2280	1760.7 (0.017)
		^{90}Zr(n,p)^{90}Y			

[a] For simplicity, the simultaneous emission of gamma particles and neutrinos during β^- decay are omitted in the reaction equations.

During recent years the interest towards the radionuclide ^{177}Lu has grown significantly due to its decay properties, radiopharmaceuticals of ^{177}Lu are finding their way to the market. Although in research the interest towards terbium isotopes has grown in recent years due to its possible benefits over the ^{177}Lu isotope. A first benefit is the fact there are 4 clinically interesting radioisotopes of Tb, two of them offering diagnostic features, ^{152}Tb emitting positrons (PET) and ^{155}Tb emitting photons (SPECT). The other two showing therapeutic capabilities, ^{149}Tb decays via α-emission with a maximum decay energy of 4.077 MeV and a half-life of 4.1 hours. ^{161}Tb decays via β^- emission with a maximum decay energy of 593 keV and a half-life of 6.91 days (Table 1).[8,9]

As can be seen in Table 1, the decay properties of ^{177}Lu are very similar to those of ^{161}Tb. ^{177}Lu has a maximum decay energy of 498 keV and a half-life of 6.65 days. Both ^{161}Tb and ^{177}Lu emit soft γ-rays suitable for SPECT imaging. However, the main benefit of ^{161}Tb compared to ^{177}Lu are the amount of Auger electrons emitted per decay. For ^{161}Tb there are about 16 times more Auger electrons emitted per decay compared to ^{177}Lu, making ^{161}Tb a promising alternative for ^{177}Lu.[10]

Low energy Auger electron emitters have a higher antitumor efficiency compared to β^- emitters due to a higher linear energy transfer (LET) on a short tissue range (Figure 1).[11] Moreover, Auger electrons have a lower toxicity when emitted outside the targeted cell. Because of their short range they can only affect the DNA when internalized inside the tumor cell.[12,13] Therapeutics by pure Auger electron emitters like ^{67}Ga and ^{111}In is limited because of the challenging targeting strategy required to reach nearby the radiosensitive targets of tumor cells. Here ^{161}Tb excels as a therapeutical radioisotope because it provides both β^- and Auger electrons.

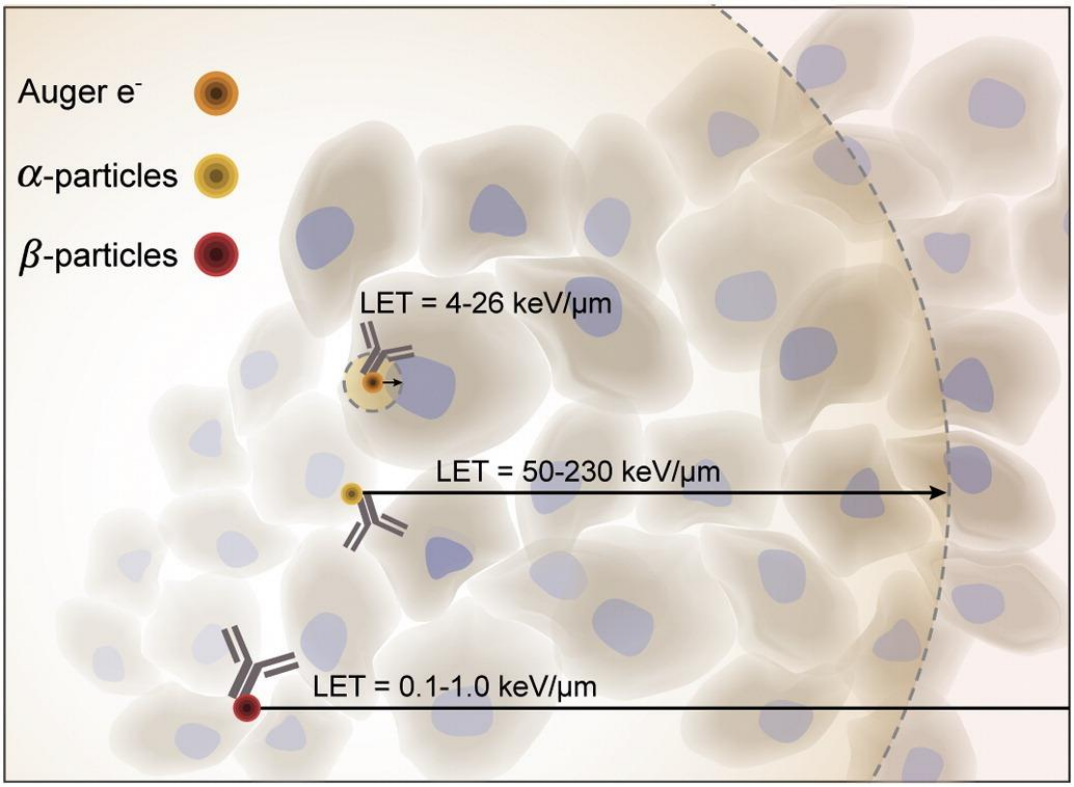

Figure 1: Path illustrations of Auger and conversion electrons, α and β^- particles.[9]

1.2. Production of medical radiolanthanides

In general radiolanthanides can be produced efficiently via two main production methods. The first method consists of the irradiation of stable lanthanides as target material by a thermal or epithermal neutron flux. These neutron fluxes originate from fission reactions in a nuclear reactor of which there are 99 research reactors (operational, under construction, temporary shutdown and planned) in 44 member states able to produce isotopes, according to the IAEA Research Reactor Base.[14] However only a fraction of these reactors are able to produce the necessary medium to high thermal neutron fluxes to produce the radiolanthanides. The advantages of nuclear reactors are the ability to irradiate a high volume, several samples simultaneously and the wide variety of radionuclides that can be produced this way.[8,9]

For the second production method of radiolanthanides a particle accelerator (cyclotron) is used to accelerate charged particles like protons, deuterons or α-particles to bombard into target isotopes. This is a production route seen for a lot of diagnostic radionuclides. Some of these diagnostic radioisotopes like ^{18}F are very unstable and neutron deficient. Due to their short half-lives, these medical radionuclides have to be produced on site. Worldwide there are more than 1200 cyclotrons used to produce medical radionuclides, making the isotopes produced in cyclotrons more accessible compared to isotopes produced via a research reactor.[8]

Since all 4 clinically interesting Tb isotopes have unstable nuclei for different reasons, also their production routes differ from each other. For ^{161}Tb, the isotope of interest in this thesis, there are two possible production routes which can be carried out by neutron capture in nuclear reactors like the BR2 research reactor at SCK CEN. The production from stable isotope ^{159}Tb requires the capture of two neutrons $^{159}\mathrm{Tb}(2\mathrm{n},2\gamma)^{161}\mathrm{Tb}$ (red, Figure 2), due to insufficient cross section, contamination by long-lived ^{160}Tb cannot be avoided. And due to the same chemical properties, purification of the wanted isotope is not an option.[5]

For the second possible production route neutron capture in a nuclear research reactor is the way. This production route is indirect: $^{160}\mathrm{Gd}(\mathrm{n},\gamma)^{161}\mathrm{Gd}\xrightarrow{\beta^-}{}^{161}\mathrm{Tb}$ (green, Figure 2). By this production route no unwanted long-lived ^{160}Tb is produced. But in this case ^{161}Tb needs to be isolated from the Gd target material and separated from its stable decay product ^{161}Dy.[5] The separation of ^{161}Tb from its target material is the main goal, of which this thesis investigates a link in the production chain. The separation of ^{161}Tb from similar lanthanides is discussed in section 3.

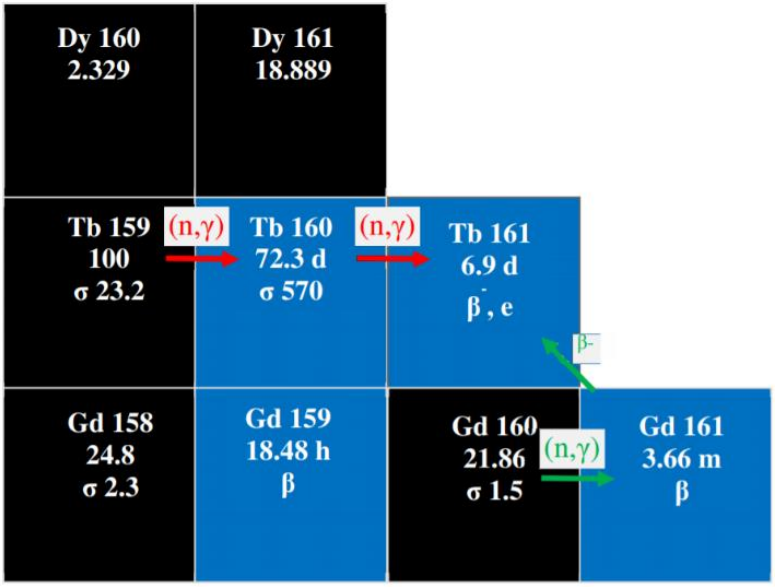

Figure 2: Cutouts of the chart of nuclides: production routes for ^{161}Tb and ^{177}Lu, direct route indicated in red and indirect route indicated in green. [6,15]

2. Coordination chemistry of terbium

Lanthanides show a wide variety in coordination numbers compared to the d-block elements. The ionic radii of trivalent lanthanides are situated between 1.032 Å (La^{3+}) and 0.861 Å (Lu^{3+}). The higher coordination numbers for lanthanides compared to transition metals can be explained by the smaller ionic radii of transition metals, with a maximum ionic radius of the transition elements for Ti^{3+} of 0.670 Å. Lanthanide ions are able to coordinate more ligands in their coordination sphere because of reduced steric hinderance. But also because f-orbitals are shielded, making them inner orbitals, what prevents them from participating in bonding. Meaning that there are no ligand-field effects preferring octahedral coordination as is observed in transition metal coordination.[16]

Lanthanides coordinated by water molecules, $[\mathrm{Ln(H_2O)_n}]^{3+}$, show coordination number 9 for the early lanthanides (La-Eu) and coordination number 8 for the later lanthanides (Dy-Lu). The intermediate elements, including Tb show a mixture of coordination numbers. Similarly as for monodentate ligands, multidentate ligands in general form 8 coordinated complexes for the later lanthanides and 9 coordinated complexes for the earlier lanthanides.[16]

Lanthanides mainly occur as trivalent cations in solution. There are however exceptions occurring in tetravalent form, Ce^{4+} and in more alkaline conditions also Tb^{4+} and Pr^{4+} were reported to occur. For Ce^{4+}, the most extensively studied tetravalent lanthanide, coordination numbers ranging from 6-12 have been found.[16,17] Still for tetravalent terbium it is a major challenge to determine the coordination number, since the formed complex is supposed to be a mixture of trivalent and tetravalent terbium.[17,18]

Varlashkin *et al*. did research towards the stability of Tb^{4+} in carbonate-hydroxide solutions.[17] The very high standard reduction potential in standard aqueous conditions (+3.1 V vs. SHE) inhibits the stabilization of Tb^{4+}. By electrolyzing Tb^{3+} in highly alkaline carbonate solution the potential necessary to oxidize Tb^{3+} is significantly lower than +3.1 V vs. SHE, allowing the stabilization of Tb^{4+}. For Ce^{4+}/Ce^{3+} a negative shift of -1.7 V has been reported for the highly alkaline carbonate solutions.[17]

In the work of Varlashkin *et al*. they mentioned that the addition of KOH is necessary to stabilize Tb^{4+} formed (electro)chemically.[17] Even a too high concentration of K_2CO_3 might lead to a tetravalent ion with no more free space for hydroxide ions to be stabilized optimally. So they state that the formed complex has to consist of both CO_3^{2-} and OH^- coordinating anions. Also they mention cluster formation where multiple Tb^{4+} and Tb^{3+} cations coordinated by both anions cluster together, however the exact ratios and form of this cluster are unknown.[17,18]

Higher CO_3^{2-} concentrations increase the needed amount of OH^- concentration to allow Tb^{3+} oxidation. When the carbonate concentration decreases, the tendency to form Tb^{4+}-precipitates increases (Table 2).[17]

Table 2: Potassium carbonate and potassium hydroxide concentrations and the influence on the stability of Tb^{4+}. Data copied from Varlashkin et al.[17]

$[K_2CO_3]$ (M)	[KOH] (M)	Stability of Tb^{4+}
1	0.15	Tb^{4+} precipitation; no Tb^{4+} solution
2	0.15	Tb^{4+} solution stable for a few hours; reduced by water to Tb^{3+}
2	0.3	Tb^{4+} precipitates from solution in about 1 h
5	0.5	Stable for weeks to precipitation or reduction by water
5	0.6	Solution slowly precipitates over a period of days to weeks

Varlashkin *et al*. tried to determine the coordination number of the formed Tb^{4+} complex by the following series of steps.[17] First separation of the Tb^{4+}-containing precipitate was done by centrifugation, then dried in vacuum at room temperature for 1 day. To measure the terbium and carbonate content, the solids were again dissolved by at least 1 M HCl, followed by dilution with water. Subsequently the pH had to be adjusted to 6. The solution was then titrated with 0.01 M ethylenediaminetetraacetic acid (EDTA) using Xylenol orange as an indicator. A weighed portion of solid was placed in a distillation flask, to which water was added (the Tb^{4+} solids are insoluble in water) and a small amount of 5 M HNO_3. Finally the solution was purged with argon gas and the formed CO_2 was passed through $Mg(ClO_4)_2$ to remove water and thereafter through a column filled with ascarite (NaOH coated silica) and $Mg(ClO_4)_2$, via the weight gain of the ascarite column, the CO_3^{2-} content in the sample could be determined according to a test with known amounts of Na_2CO_3. However, this experiment was no success since the determined terbium content in the solids was not constant but varied between 61% and 68%. The amount of time the solids are dried had no influence, so the weight variation is probably not due to adsorbed water. They suggested it might be due to a different degree of hydration or complexation by water.[17]

3. Separation processes for lanthanides

Separation of neighboring lanthanides from a solution is a difficult challenge to overcome as they have similar chemical properties due to their similar ionic radii and trivalent state in solution. The three different separation techniques which were researched for the separation of ^{161}Tb are: extraction chromatography, ion-exchange chromatography and solvent extraction.[16]

3.1. Extraction chromatography

Lanthanide separation via extraction chromatography has been extensively studied by Horwitz *et al*.[6,19] This technique has a lot of potential as it combines the selectivity of liquid-liquid extraction and the ease of use with the multistage character of chromatography techniques. Tb/Gd separation reaches the highest separation factor for neighboring lanthanides with acidic extractant, 2-ethylhexylphosphonic acid mono-2-ethylhexyl ester (HEH[EHP]).[6] Monroy-Guzman *et al*. reported a very good separation for micro-amounts of daughter nuclide ^{161}Tb in macro-amounts of parent target Gd via extraction chromatography with Di-(2-ethylhexyl)phosphoric acid (HDEHP) loaded on inert polymeric absorbent (syndiotactic polystyrene resin).[20]

In Figure 3 it is shown that the ^{161}Tb/Gd couple has the highest separation factor compared to daughter/parent couples: ^{149}Pm/Nd, ^{166}Ho/Dy and ^{177}Lu/Yb. The separation factors are shown as a function of the logarithm of the HNO_3 concentration. HNO_3 is used as the acidic mobile phase.[20]

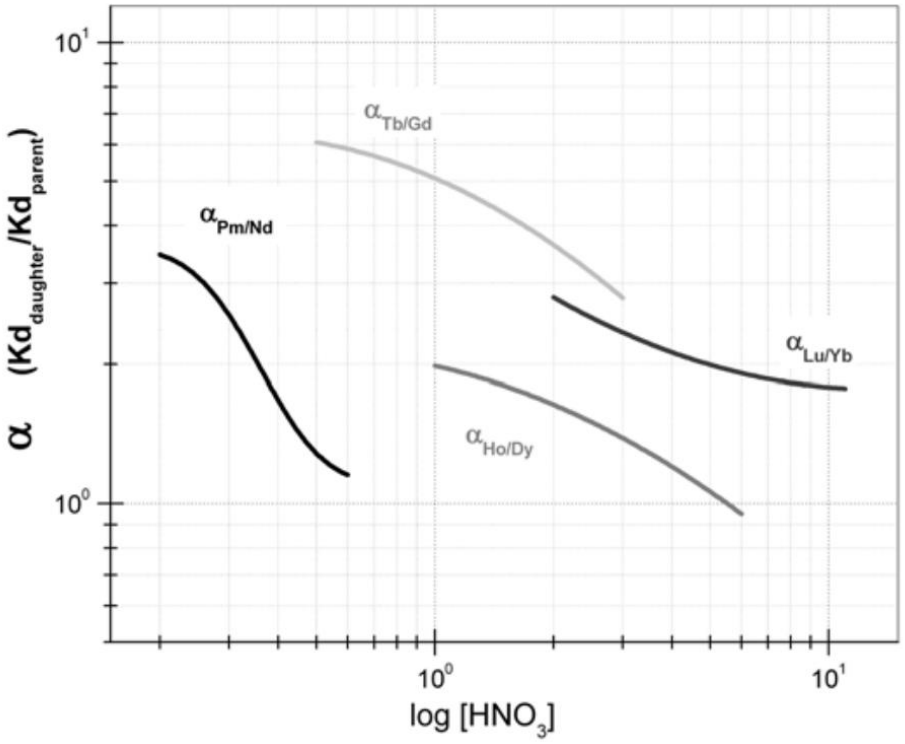

Figure 3: Extraction chromatography: separation factors (α) of lanthanide couples ^{161}Tb/Gd, ^{149}Pm/Nd, ^{166}Ho/Dy and ^{177}Lu/Yb in Ln SPS Eichrom resin as a function of $[HNO_3]$.[20]

However some serious disadvantages occur at extraction chromatography, it is very time-consuming, produces a lot of nuclear waste as the target material which is present in large amounts elutes before the target nuclide and a lot of eluent is necessary.[21,22] Also Mikolajczak

reported that the purity achieved after extraction chromatography is too low for radiopharmaceutical purposes.[6,23,24]

3.2. Ion-exchange chromatography

Ion-exchange chromatography is widely implemented for nuclear radionuclides separation and purification.[25] In Figure 4 the gradient elution of pressurized ion-exchange chromatography performed by Campbell *et al*. is shown.[26] Figure 4A shows the elution bands and Figure 4B shows the increasing concentration of eluent during chromatography. An initial conclusion extracted from Figure 4A: Tb was eluted before Gd, the target material, minimizing the nuclear waste compared to extraction chromatography.[26]

Initial ion-exchange chromatography took several days to separate rare earths on large scale. Campbell *et al*. succeeded in quantitative separation after 1 to 2 hours of pressurized ion-exchange chromatography with a Dowex 50W-X8 ion exchange resin and an increasing concentration over time of the eluent, α-hydroxyisobutyrate solution.[26] To optimize the separation in a minimal time frame, the concentration gradient is probably the most important variable (Figure 4). The concentration gradient was kept constant right before the elution of the more difficult to separate couples like Lu/Yb, Gd/Eu and Pm/Nd. The least efficient separations were obtained when separating at room temperature or when increasing the column load to about 10% of the resin, even when simultaneously reducing the flow rate and using a less steep eluent concentration gradient. Increasing the column length had no significant effect, nor had the increase of the column diameter.[26]

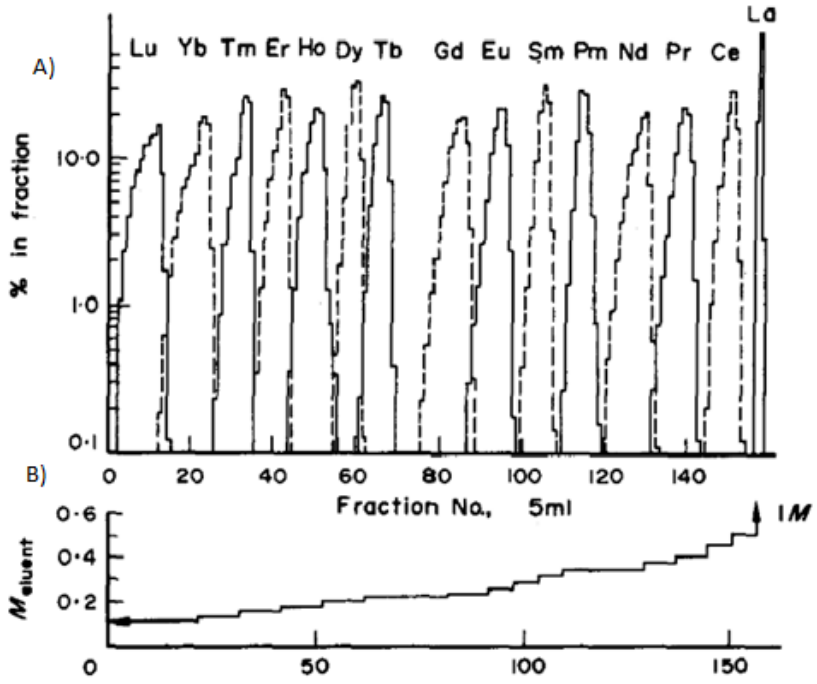

Figure 4: Pressurized ion-exchange chromatography: gradient elution of lanthanides at 80°C; 33 cm long and 0.9 cm wide column; low column loading conditions; eluent, α-hydroxyisobutyrate (pH 4.4); flow rate, 10 mL/min A) Showing the elution bands. B) Showing the increasing concentration of eluent during chromatography. Figures copied from Campbell et al.[26]

However there still are some disadvantages: impurities in the Tb-fraction occur due to a large amount of eluent needed in the cation exchanger. Ionizing radiation can influence the ion resin of the column leading to a decrease in exchange capacity and swelling. Cation exchangers are more stable to deterioration than anion exchangers.[23] Also for these previous techniques the column load must be limited to achieve a decent separation.

3.3. Solvent extraction

More efficient separation techniques can be based on the separation of different oxidation states of lanthanides, by oxidizing specific element prior to the separation step. When elements are in different oxidation states the separation is facilitated significantly. Qiang *et al*. reported solvent extraction characteristics of Tb^{4+}/Tb^{3+} periodate complexes with quaternary ammonium salts.[6,23,24,27] After oxidation of Tb^{3+} by ozonolysis, the extraction is carried out using a quaternary ammonium chloride, tricaprylmethylammonium chloride, also called aliquat-336 as the organic phase. Analyzing the Tb concentrations of both oxidation states in aqueous phase before and after extraction made it possible to determine the extraction yield (E%) and the distribution ratio (D) of Tb^{4+} and Tb^{3+} periodate complexes. The influence of several parameters has been measured in this way, including the concentration of the extractant, the

organic/ aqueous phase ratio, the pH of the stock solution, the addition of salting-out agent KNO_3, the influence of the extractant form, the diluent and the extraction time. Qiang *et al*. came to the following conclusions, an increase in extractant concentration lead to an increase in both E% and D. The results for the influence of the extractant concentration are shown in Table 3.[23]

Table 3: Solvent extraction: influence of solvent concentration on extraction yield (E%), distribution ratio of Tb^{3+} and Tb^{4+} (D) and separation factor (β).[23]

Extractant Concentration (vol%)	E(%)		D		β
	Tb^{3+}	Tb^{4+}	Tb^{3+}	Tb^{4+}	
20	43.6	71.7	0.773	2.53	3.27
25	47.9	74.3	0.919	2.89	3.14
30	56.4	82.1	1.29	4.59	3.56
35	60.2	86.2	1.51	6.25	4.14
40	72.5	95.1	2.64	19.4	7.35

The solvent extraction technique on its own is not a very efficient technique to separate different lanthanides of the same trivalent oxidation state. It requires an oxidation or reduction step in advance to separate different oxidation states to maximize its efficiency or by going for the more advanced technique which simultaneously relies on chromatographic techniques.

4. Lanthanide oxidation states

Lanthanides mainly have the following electron configuration $[Xe]4f^n6s^2$ at oxidation state 0. However for La, Ce, Gd and Lu one electron finds itself in the 5d-orbital. All elements of this group mainly occur as trivalent cations, which translates in losing two electrons from the 6s-orbital and one electron from the 5d- or 4f-orbital, leading to a new electron configuration $[Xe]4f^m$.

By forming an empty, half-filled or filled 4f orbital, different oxidation states from 3+ are formed. Only Eu^{2+} and Ce^{4+} are to a certain extent stable in aqueous solution at neutral pH, however the conditions of the solution can be manipulated to allow oxidation or reduction of some other lanthanides. Tb^{4+} isn't stable in aqueous solution at neutral pH because of the high reduction potential of Tb^{4+}/Tb^{3+} = +3.1 V vs SHE,[28] compared to the standard reduction potential of Ce^{4+}/Ce^{3+} = +1.7 vs SHE.[28] The aqueous conditions need to be enhanced to stabilize Tb^{4+}. The extension of the potential window allows Tb^{3+} oxidation. The degree of complexation of the metal by various anions present in solution, has an influence on the Ln^{4+}/Ln^{3+} reduction potential. When certain complexes favor to be formed with the tetravalent lanthanide state instead of the trivalent form, this will lower the reduction potential.

The oxidation of Ce^{3+} is more extensively researched compared to Tb^{3+} oxidation, because of the more accessible redox potential of Ce^{3+}. The following sections will also discuss Ce^{3+} oxidation since it has been shown that certain conditions which favor Ce^{3+} oxidation also favor the oxidation of Tb^{3+}.[27]

4.1. Oxidation in aqueous medium

For both Ce^{3+} and Tb^{3+} successful oxidation and stabilization has been shown. Because of the easier to realize oxidation more knowledge has been obtained and on its turn implemented in the research towards oxidation of Tb^{3+} and the stabilization of Tb^{4+}.

4.1.1. Electrochemical oxidation of Ce^{3+} in aqueous medium

Hobart *et al*. had shown successful oxidation of Ce^{3+} and stabilizing its tetravalent form in aqueous solutions of phosphoric acid and alkali metal carbonates.[27] To qualitatively indicate the oxidation of Ce^{3+} has successfully been achieved, the absorption spectra are measured. In Figure 5 spectra for both Ce^{3+} and Ce^{4+} are shown, the oxidized form shows a broad absorption peak with a maximum of about 320 nm. The oxidation of Ce^{3+} also visibly changes the solutions color, from colorless to pale yellow. [27]

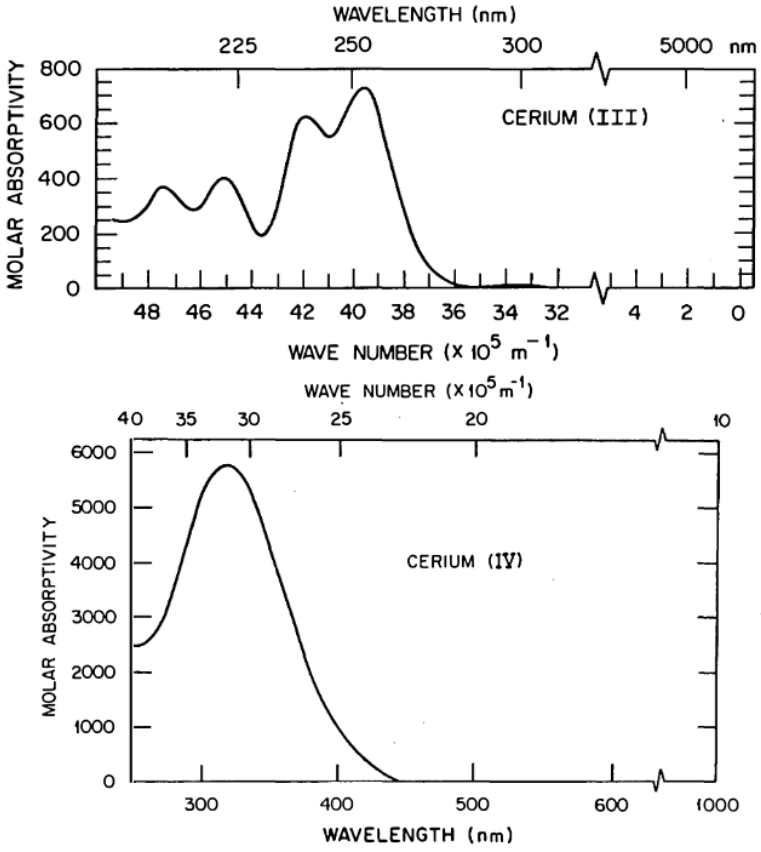

Figure 5: Absorption spectra of Ce^{3+} and Ce^{4+} respectively in 1 M $HClO_4$ and 1 M H_2SO_4.[27]

In a solution of 15 M H_3PO_4 the standard reduction potential of Ce^{3+}/Ce^{4+} = +1.7 V, has been lowered by +1 V making it possible to oxidate Ce. However the lowering of reduction potential is insufficient for the oxidation of Tb^{3+}.[27]

An interesting observation was made by Hobart *et al*; preparing a mixture including Ce^{3+} salt and K_2CO_3 resulted in a color change of the solution surface in a few minutes time.[27] This change of color indicates the formation of Ce^{4+} due to the oxidation by atmospheric oxygen. This indicates a big change in reduction potential when using a 5.5 M K_2CO_3 solution. Assuming a similar reduction potential change, concentrated potassium carbonate also would allow the oxidation of both terbium and praseodymium.[27]

4.1.2. Electrochemical oxidation of Tb^{3+} in aqueous medium

When Hobart *et al*. implemented the 5.5 M K_2CO_3 solution into the Tb^{3+} oxidation, color change from colorless to golden-brown was observed at the Pt working electrode when applying +1.3 V vs. SHE , indicating Tb^{3+} oxidation to Tb^{4+}.[27] The color dissipates in the bulk of the solution, to maintain the color in bulk or to stabilize the formed Tb^{4+}, 1 M of KOH has to be added. Also for the oxidation of Tb^{3+} qualitative indications can be shown by absorption spectroscopy. Figure 6 shows the absorption spectra of both Tb^{3+} and Tb^{4+} in concentrated potassium carbonate solution, similar to Ce^{3+} oxidation a characteristic broad band appears upon oxidation, with a maximum absorption at 365 nm.[27]

Electrochemical oxidation of Tb^{3+} also has been done successfully by an applied potential of +1.3 V in solutions of 5 M Cs_2CO_3 and 2 M Na_2CO_3, both at pH 14. The absorption spectra for different solutions gave similar absorption bands as in 5.5 M K_2CO_3. They observed it was necessary to use platina electrodes because glassy carbon (GC) electrodes were not inert at applied voltages above +1 V in solutions of pH 14. [27]

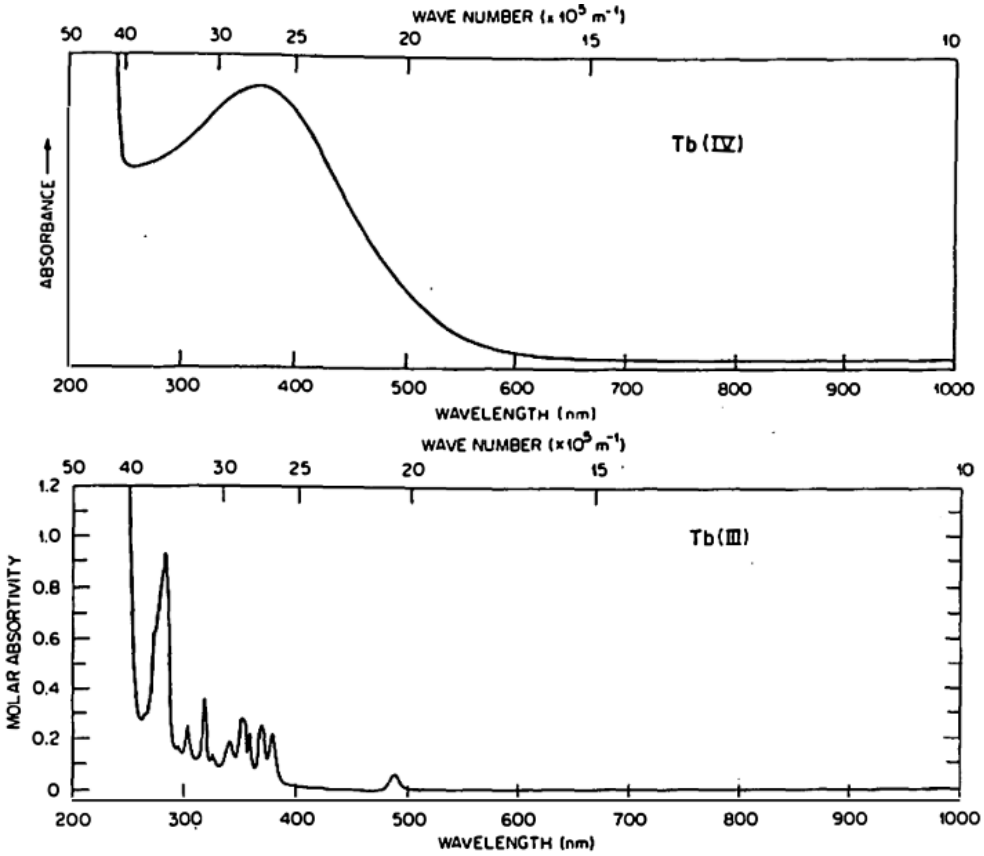

Figure 6: Absorption spectra of Tb^{3+} and Tb^{4+}, both in 5.5 M K_2CO_3.[27]

Varlashkin *et al*. carried out similar oxidation experiments to the ones done by Hobart *et al*.[17,27] They also succeeded in the oxidation of Tb^{3+} electrochemically by applying over +1 V with a platina working electrode. For different concentrations of K_2CO_3 and KOH in water they evaluated the stability of the formed Tb^{4+}. For the results on this stability experiment see the chapter on coordination chemistry. However a problem they encountered was the formation of a brown film on the platina working electrode, which reduced the surface area and consequently reduced the oxidation rate. They had the same absorbance peak around 365 nm indicating Tb^{4+} present in solution.

Propst *et al*. attempted Tb^{3+} oxidation with a conducting glass electrode (CGE) in a solution of 0.5 M KOH and 2.5 M K_2CO_3 and varying Tb-salt concentrations depending on the experiment.[18] They found that oxidation did occur, but overall Tb^{4+} has a complex electrochemistry. The solution contains a form of electro-active and -inactive forms of trivalent terbium which are in equilibrium with each other. Also they witnessed a polymerization of the formed tetravalent terbium. Reduction of Tb^{4+} occurred in solid state, leading to an intermediate with mixed oxidation state $Tb_2^{3.5+}$ which on its turn was in equilibrium with Tb^{4+} and Tb^{3+} in solid state.[18]

4.1.3. Chemical oxidation of Tb^{3+} in aqueous medium

Both Hobart *et al*. and Xiaojing *et al*. were able to oxidize Tb^{3+} to its tetravalent state via chemical oxidation with ozone as strong oxidizing agent (standard reduction potential of ozone +1.246 V).[27,29] Both using different solutions but adjusted pH to 14.[29]

Hobart *et al*. used the same solution as they found to be optimal for the electrochemical oxidation of Ce and Tb: 5.5 M K_2CO_3 and pH adjusted to 14. They did not report about the characterization and optimal conditions in addition to indicating they succeeded by measuring the absorption spectra. [27]

Xiaojing *et al*. reported the chemical oxidation of Tb^{3+} in an aqueous solution of tetrametaphosphate by ozonolysis.[29] They measured absorbance peaks similar to the ones in Figure 6 reported by Hobart *et al*.[27] They examined both the oxidation rate and the stability of Tb^{4+}. To get an indication of the stability they measured the reduction rate, since the oxidation and reduction are in equilibrium with each other, meaning a higher reduction rate corresponds to a lower stability. They varied parameters such as pH and temperature of the solution, initial concentration of Tb^{3+} and the concentration of tetrametaphosphate.[29]

They found that the pH had an optimal window between pH 11 and 12.7. For a pH<11 the reduction potential of Tb^{4+}/Tb^{3+} is still too high, making oxidation of Tb^{3+} impossible in aqueous solution. When pH>13 they observed the Tb^{3+} - $P_4O_{12}^{4-}$ complex became unstable preventing the lowering of the reduction potential. It is concluded that inside the optimal pH-range, a higher pH correlates to a higher oxidation rate of Tb^{3+} and a better stability of Tb^{4+}. In Table 5 the increased stability or reduced Tb^{4+} reduction rate for higher pH is shown. [29]

Table 4: Reduction rate of Tb^{4+} for different pH values of solution, other parameters are kept constant. (Indicating the stability of the formed Tb^{4+})[29]

pH of solution	Reduction rate constants 10^6k (s^{-1})
11.20	60.8
11.40	22.8
12.00	5.42
12.56	3.57

When the pH is kept constant the temperature has a significant influence on the generation rate and stability of Tb^{4+}. The oxidation has to be seen as an equilibrium where simultaneously reduction of Tb^{4+} to Tb^{3+} occurs; at increasing temperature the rates of both oxidation and reduction are increased, however also meaning the stability is shifted towards the reduced

form at higher temperatures. So lower temperatures are more beneficial for oxidation, in particular the stabilization of Tb^{4+} as indicated in Table 5.[29]

Table 5: Reduction rate of Tb^{4+} for different temperatures of solution, other parameters are kept constant. (Indicating the stability of the formed Tb^{4+})[29]

Temperature of solution (°C)	Reduction rate constants 10^6k (s^{-1})
53.0	85.5
44.0	59.2
36.0	27.7
27.5	10.8
15.0	5.42
6.5	3.33

Because the concentration of ozone bubbled through the solution is constant and can't be increased limitlessly, there is a maximum of initial Tb^{3+} concentration that can be oxidized at a time. Also for the concentration of tetra metaphosphate the influence was negligible compared to the other parameters.[29]

Varlashkin *et al*. have next to electrochemical oxidation, also conducted experiments by chemical oxidation with ozone.[17] The results for their stability experiment of Tb^{4+} doesn't differ when the oxidation is done electrochemically or chemically, because the resulting Tb^{4+}-solution is the same. But they reported the oxidation happened faster and was more convenient (especially for larger volumes of solution) when done chemically, compared to when done electrochemically. According to Varlashkin *et al*. this was due to formation of a "brown film" on the platina working electrode when oxidizing electrochemically.[17]

4.2. Oxidation in organic medium

Organic media are less extensively studied compared to aqueous media, because the separation after oxidation is more complex for organic media. Due to the limited conductivity, salts need to be added to solve these problems, however at the end this makes an extra component where the tetravalent terbium needs to be purified from. Also studies showed the oxidation of lanthanides is solvent dependent.[30]

Payne *et al*. did research towards the solubility and oxidation of Ce, Tb and Pr, which had been oxidized earlier in successful (aqueous) conditions.[30] They used lanthanide nitrates and lanthanide chlorides in the presence of oxygen donor ligands triphenylphosphine oxide (TPPO) and triphenyl arsine oxide (TPAsO), using acetonitrile as solvent.[30]

They attempted chemical oxidation via ozonolysis or by air/oxygen gas purging at an increased temperature of 70°C for Ce^{3+}, Tb^{3+} and Pr^{3+}. For cerium all 4 combinations of the two different donor ligands and oxidation by either air/oxygen or ozone showed successful oxidation to a certain extent in the way of color change of the solution. For both terbium and praseodymium the only combination which has shown a sign of oxidation after 4 hours is the use of TPAsO as oxygen donor ligand while oxidizing by purging ozone.[30]

Table 6: Observations and interpretations from Payne et al. of the oxidation of Ce, Pr and Tb in the presence of oxygen donor ligands. Table copied from Payne et al.[30]

Lanthanide	TPPO with air and/or oxygen	TPPO with ozonolysis	TPAsO with air and/or oxygen	TPAsO with ozonolysis
$Ce(NO_3)_3.6H_2O$	Very faint pale yellow solution of Ce^{4+}	Pale yellow solution of Ce^{4+}	Yellow solution of Ce^{4+}	Purple-brown solution, possibly mixed-valence Ce^{3+} and Ce^{4+}; no change on standing
$CeCl_3.6H_2O$	No reaction[b]	[a]	Yellow-orange solution of Ce^{4+}	[a]
$Pr(NO_3)_3.6H_2O$	No reaction	No reaction	No reaction	Golden solution of Pr^{4+} after 4 h
$PrCl_3.6H_2O$	No reaction	[a]	No reaction	[a]
$Tb(NO_3)_3.6H_2O$	No reaction	No reaction	No reaction	Yellow solution of Tb^{4+} after 4 h
$TbCl_3.6H_2O$	No reaction	[a]	No reaction	[a]

[a] Ozonolysis of lanthanide chlorides was not attempted since ozone would oxidize the Cl^-.

[b] No reaction = no observation after at least 4 h of ozonolysis, 1 h of bubbling oxygen or left standing overnight.

Except for one attempt of electrochemical oxidation of Ce in molten dimethyl sulfone by Varlashkin and Peterson, which had a slow oxidation rate and poor characterization, the attempts of Ce^{3+} oxidation in organic media are limited.[6,31–33]

4.3. Tb^{4+} Quantification in aqueous carbonate solutions

The most convenient technique would be UV/VIS absorbance because it's been determined that Tb^{4+} complex in carbonate solution has a broad absorbance peak with a maximum around 360 nm which is not observed for Tb^{3+}.[27] However to use the formula of Lambert-Beer the molar absorptivity (Ɛ) of Tb^{4+} is needed.

Hobart *et al*. determined an estimated value for the molar absorptivity of the 360 nm absorbance band to be larger than 1000 $M^{-1}cm^{-1}$.[27] The way they estimated this was by preparing various solutions with partially oxidized Tb. For these solutions they correlated the decrease in absorbance values measured for a Tb^{3+} absorbance peak with a known molar absorptivity, with the increase in absorbance values for the absorbance peak corresponding to Tb^{4+}.

The quantitative method attempted by Varlashkin *et al*. to determine the molar absorptivity of Tb^{4+} is a redox titration.[17] From all the titrants tested, ferrocyanide $Fe(CN)_6^{4-}$ was the most promising as it was able to reduce Tb^{4+}. Although quantification was not possible since as a first issue they stumbled upon, the Tb^{4+} complex was slowly precipitating in their 3 M K_2CO_3 with 0.25 M KOH solution. And as a second problem they observed the redox titration was not a simple one-electron exchange between Fe^{2+} and Tb^{4+}.[17] Aside from the occurred problems they were able to make an estimation for the molar absorptivity of Tb^{4+} in carbonate solutions, by following the redox titration with UV/VIS absorbance measurements. Their estimated molar absorptivity was found to be about 1000 $M^{-1}cm^{-1}$, which is similar to the one estimated by Hobart *et al*.[27] No exact determination of the molar absorptivity for Tb^{4+}-carbonate complex was succeeded yet. [17,27]

II. Goals and objectives

The main goal of this thesis is to investigate the electrochemical oxidation of Tb^{3+} in aqueous carbonate solution and optimize the yield of Tb^{4+}. The oxidation of Tb^{3+} is a step performed to facilitate the separation of ^{161}Tb from the ^{160}Gd target material in the production process. The oxidation is done electrochemically because of multiple reasons, it is a clean process where no extra chemical substances are added which afterwards need to be separated again. In electrochemical oxidation, the applied potentials can be set very precise, where at chemical oxidation this depends on the chosen oxidizing agent.

Tb^{4+} reduction is investigated with the goal of indirectly quantifying the formed Tb^{4+} from electrochemical oxidation of Tb^{3+}. Subsequently from this electrochemical quantification, the molar absorptivity (ε) of the Tb^{4+} complex for the absorbance band around 360 nm can be determined.

The next goal is to investigate the influence of several parameters on the electrochemical oxidation of Tb^{3+} in aqueous carbonate solutions. The chosen parameters are the concentrations of Tb and K_2CO_3 in solution, the pH of the solution and the temperature of the solution. For the concentrations of Tb, more Tb^{4+} is expected to be formed for increasing Tb concentrations up until the concentration where Tb precipitates start to form. For the pH of the solution it is investigated to what extent the electrochemical oxidation of Tb^{3+} would still occur upon deviating the pH from 14. From the results determined by Xiaojing *et al*. it was found that electrochemical oxidation was most efficient for lower temperatures.[29] However these experiments were performed in a tetrametaphosphate solution, while in this work the temperature influence is determined for a carbonate solution.

As a final goal different types of electrochemical cells are examined to determine the possibilities of different electrolytic systems for the electrochemical oxidation of Tb^{3+} in aqueous carbonate solution. The possibility of oxidizing Tb^{3+} in a divided cell, where the counter electrode is placed in a separate compartment isolated from the rest of the cell by different semi-permeable membranes, is investigated. For the divided cell the possible back reduction of Tb^{4+} would be excluded, leading to higher efficiencies. Also the oxidation of Tb^{3+} in a so-called flow cell, where the solution flows past the electrodes, is examined for several parameters. The ratio of working electrode surface area versus volume of solution is expected to increase the overall oxidation rate. The residence time of solution in the cell is expected to have a big influence, as the residence time should be long enough to oxidize a sufficient amount of Tb^{3+}. In standard bulk electrolysis cells the mass transport is due to diffusion, in the

flow cell the mass transport is assisted by the applied flow, expected to have a positive influence on the oxidation rate.

III.Safety, Health and Environment

When working in a chemical laboratory everyone performing any experiment should be conscious of what he or she is performing and know the accompanied risks that come with these experiments. Therefore, making a risk analysis of all harmful chemicals and potentially dangerous techniques is a must before executing any experiment. In this way proper precautions can be taken to minimize the risk of harming oneself, others and environment. For all experiments the standard personal protective equipment was worn e.g. lab coat, nitrile gloves and safety goggles. A fume hood was used when dangerous gasses could occur or when working with highly concentrated acids. In the following section the risks of used chemicals are mentioned and the necessary precautions coming with these risks.

The three salts necessary to prepare the standard aqueous Tb^{3+} solutions are terbium trichloride hexahydrate ($TbCl_3 \cdot 6H_2O$), potassium carbonate (K_2CO_3) and potassium hydroxide(KOH). All three salts cause skin irritation and eye irritation. KOH causes severe skin burns and eye damage and also may be corrosive to metals. So at any skin contact of the salts it should be immediately rinsed with plenty of water.

Nitric acid (HNO_3) is used to clean platina electrodes in between the experiments. It may intensify fire, as it is classified as an oxidizer. May be corrosive to metals and causes severe skin burns and eye damage. Also it is toxic if inhaled, so all actions with nitric acid should happen in a fume hood.

Diluted sulfuric acid (H_2SO_4) is used to measure cyclic voltammetry measurements with platina electrodes. The concentrated acid may be corrosive to metals and causes severe skin burns and eye damage. So when diluting the concentrated acid, handle with extreme care and under a fume hood.

Also care should be taken of the waste produced in the experiments. The waste generated in the experiments is either alkaline aqueous or acidic aqueous, which either must be sorted and collected in the waste bins associated.

IV. Experimental

1. Materials

1.1. Reagents and sample preparation

As Tb^{3+} source, $TbCl_3 \cdot 6H_2O$ (99.9%) was purchased from Strem Chemicals, Inc. (Newburyport, USA). K_2CO_3 (anhydrous,≥ 98%) and KOH pellets were purchased from VWR International B.V. (Leuven, Belgium). HNO_3 (65%) was purchased from Sigma-Aldrich BVBA (Overijse, Belgium). H_2SO_4 (95-97%) was purchased from Sigma-Aldrich BVBA (Overijse, Belgium). All chemicals were used as received without any further purification. All aqueous solutions were prepared with ultra-pure water (18.2 MΩ cm at 25 °C).

The Tb^{3+} solution used in bulk electrolysis consisted of 70 mM $TbCl_3 \cdot 6H_2O$, 4 M K_2CO_3 and 75 mM KOH giving pH 14. These concentrations were determined in the parameter study and were used for all further experiments which required a Tb^{3+} solution. Also it was found the order of dissolving the salts was important, first the Tb-salt, followed by the K_2CO_3 and at last the KOH. Also, all added salt had to be dissolved before adding the next reagent, otherwise terbium-hydroxide precipitates might form. If necessary an ultrasonic bath was used to help the salts dissolve easier. The pH of the solutions was determined with the DG111-SC KCl 3 M combined glass pH electrode of a Mettler Toledo Excellence Titrator T5.

1.2. Working electrode types and materials

At the working electrode (WE) the redox reaction of interest occurs. Before and after any experiment the electrode surface had to be cleaned thoroughly, because electrolysis is very sensitive to contamination of the electrodes. The material of the working electrode has to be redox-inert at the potentials at which they are used.

Depending on the application, different types of electrodes were used as working electrode. For bulk electrolysis Pt working electrodes were used to oxidize Tb^{3+}. When in a large setup of 50 mL the large Pt gauze (NM-D001) from BASi was used, for which a surface area of 140 cm^2 has been estimated, although only half the electrode surface was submerged in a 50 mL solution. When in small volume setup of 5 mL a small Pt mesh, with an estimated surface area of 20 cm^2, was used as the working electrode. The flow cell has its own type of Pt working electrodes (MF-1031) from BASi, for both type of flow cells have a surface area of 7.1 mm^2. For the cyclic voltammetry experiments both Pt (MF-2113) and glassy carbon (MF-2012) standard disc electrodes from BASi were used as a working electrode, both have a surface area of 7.1 mm^2. For reduction in bulk a reticulated vitreous carbon (RVC) electrode (MF-2077) from BASi has been used as a working electrode with an estimated surface area of 1000 cm^2.

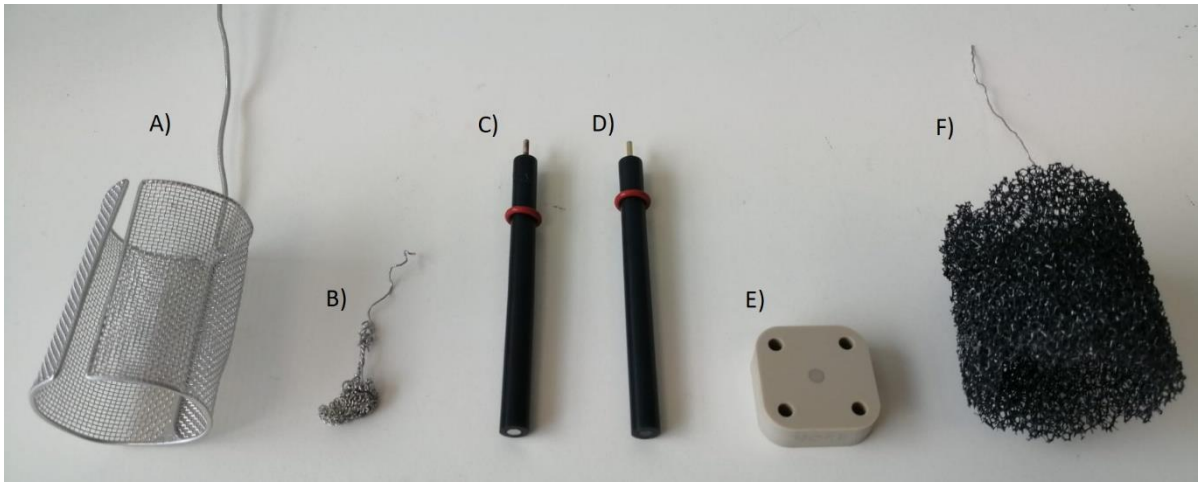

Figure 7: Electrodes used as working electrode: A) large Pt gauze. B) Pt mesh. C) standard Pt disc. D) standard glassy carbon disc. E) flow cell Pt working electrode. F) reticulated vitreous carbon (RVC).

1.3. Counter electrodes types and materials

To close the electrical circuit a counter electrode (CE) or auxiliary electrode is used. At the counter electrode an equally large current but with reversed sign occurs, compared to the current measured at the working electrode. In some situations it might be possible that undesired reactions occur at the counter electrode, for example the formation of a dangerous gas or a species which might interact with the wanted product formed at the working electrode. To prevent these undesired reactions from happening in the same solutions as the wanted reactions at the working electrode, the counter electrode can be separated from the solution by a semipermeable barrier. The use of such a semipermeable barrier was also tested for the reactions in this thesis.

As a counter or auxiliary electrode for all experiments, except for the flow cell experiments, a Pt coil or Pt wire electrode were used. For the flow cell the outlet or the bulk metal cell function as a counter electrode.

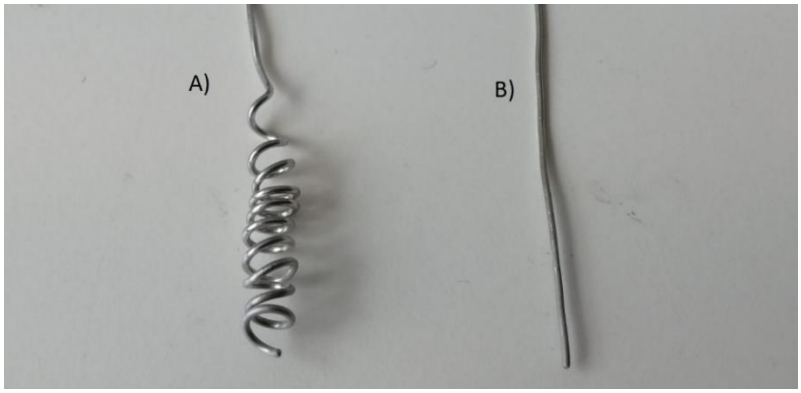

Figure 8: Different electrodes used as counter electrode: A) Pt coil. B) Pt wire.

1.4. Reference electrodes

When a defined potential is applied for certain experiments, a reference electrode is necessary to make sure the applied potential is accurate. The potential at the reference electrode is used as a reference point to determine the exact applied potential at the working electrode. As the reference electrode determines what potential is applied in the cell it is very important the electrode is in a good state and stored correctly. The potential of the standard hydrogen electrode (SHE) is determined to be zero at all temperatures.

For all electrochemical experiments, the same type of reference electrode has been used, the Ag/AgCl in 3M KCl reference electrode (+0.210 V vs. SHE). For all electrochemical experiments, except the ones with the flow cell, the long reference electrode with CoralPor® porous frit (MF-2056) from BASi was used. The flow cells have their own reference electrodes which tightly fit into the cell. For the radial flow cell a reference electrode with porous ceramic frit (MW-2030) from BASi has been used and for the cross flow cell one with a different connection, but also with a porous ceramic frit (ALS-Japan: 013488).

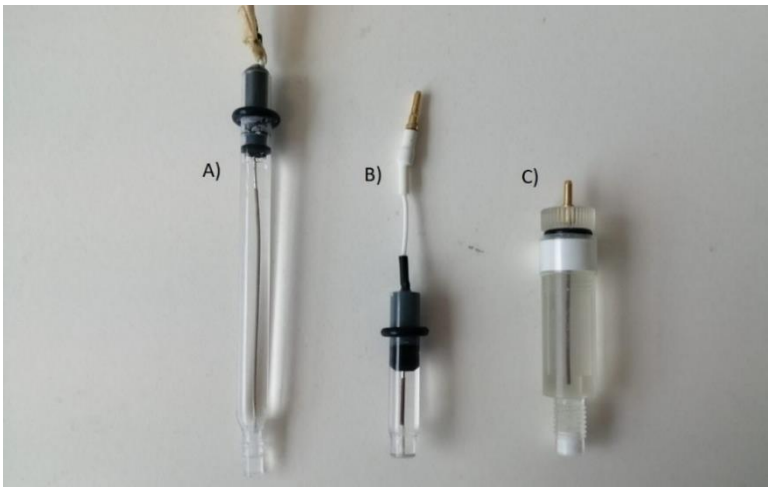

Figure 9: Reference electrodes used: A) reference electrode with CoralPor® frit. B) reference electrode for radial flow cell. C) reference electrode for cross flow cell.

2. Methods

2.1. Bulk electrolysis

At controlled potential bulk electrolysis, a constant potential was applied in a three electrode configuration for a defined amount of time. The current response was measured over time with the intention of oxidizing or reducing Tb^{3+} or Tb^{4+} respectively in solution. The applied potential was maintained steady by the use of a Ag/AgCl reference electrode as mentioned before.

For the electrochemical experiments, there were two types of potentiostats available. These were an Autolab PGSTAT302N with a compliance voltage of 30 V and a current range up to 2

A and an Autolab PGSTAT204 with a compliance voltage of 20 V and a current range up to 400 mA. Both instruments were controlled with an external PC using software Nova 2.1.4 from Metrohm Autolab.

The oxidation of Tb^{3+} has been done both in a small volume setup of 5 mL and in a large volume setup of 50 mL. The same salt concentrations were used for the small and large setup. The three electrodes used in both setups are mentioned above in the section about the electrodes. Both the working and counter electrode were Pt electrodes.

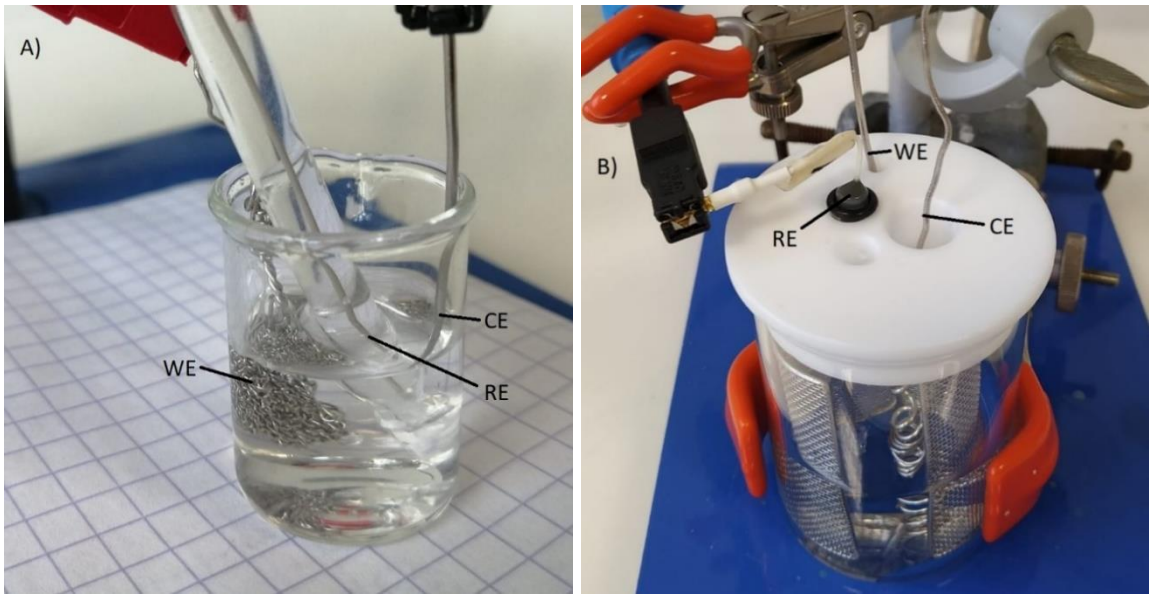

Figure 10: Both setups for bulk electrolysis oxidation with the working electrode (WE), Counter electrode (CE) and reference electrode (RE) indicated in the picture: A) The small volume (5 mL) setup in a 10 mL beaker. B) The large volume (50 mL) setup in a 100 mL cell.

Also the influence of the solutions temperature on Tb^{3+} oxidation has been determined by the use of a cell equipped with an external water jacket (Figure 11) and a Polyscience Digital Temperature controller 9101. Since it took a while for the solution to reach the temperature of the external waterflow, the solution was left in the cell for about 30 minutes before experiments were performed.

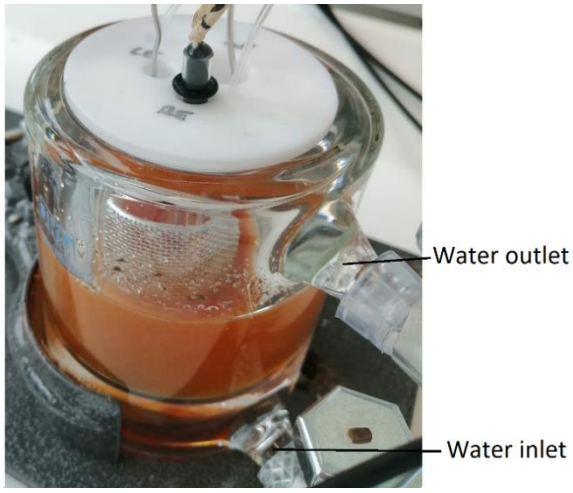

Figure 11: Bulk electrolysis cell equipped with a water jacket to regulate the solutions' temperature via an external waterflow.

The reduction of Tb^{4+} was done in batches of 20 mL. As a working electrode a reticulated vitreous carbon (RVC) electrode was used and the same coil Pt counter electrode is used in the reduction as in the oxidation experiments. Tb^{4+} solutions were prepared by applying +1.3 V vs. Ag/AgCl in 3 M KCl, using the Pt gauze working electrode in 50 mL of Tb^{3+} solution for 2 hours.

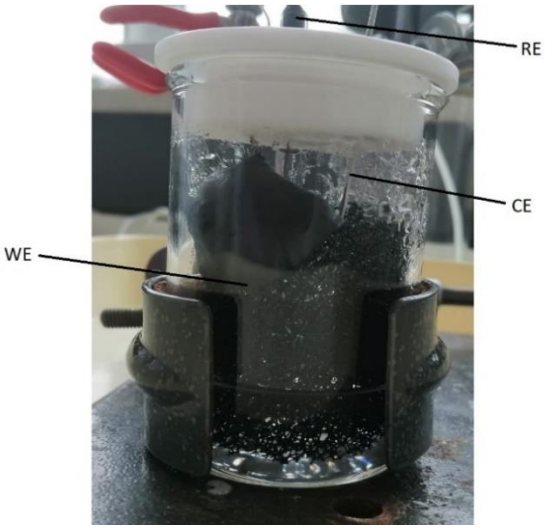

Figure 12: Tb^{4+} reduction setup with the working electrode (WE), Counter electrode (CE) and reference electrode (RE) indicated in the picture

2.2. Electrochemical impedance spectroscopy (EIS)

EIS is a widely implemented technique to analyze electrochemical systems. The resistance solely caused by the electrolyte solution is measured at high frequencies (~20 kHz) in the EIS spectrum, since generally no electrochemical phenomena occur at the high frequency range. The resistance generally is a result from the conductivity of the used solvent with present

electrolytes. Another factor with influence on the resistance is the distance between the working and counter electrodes. For the EIS measurements only the earlier mentioned, Autolab PGSTAT302N could be used, because for the impedance measurements the frequency response analysis module (FRA32M) is necessary, but was not present in the Autolab PGSTAT204.

The EIS measurements were used in experiments regarding the divided cell, where the counter electrode was separated by a semi-permeable membrane from the rest of the cell. The two tested membranes were a standard counter electrode chamber with a porous glass frit (MR-1196) from BASi and a CoralPor® frit attached to a chamber similar to those for reference electrodes, also from BASi.

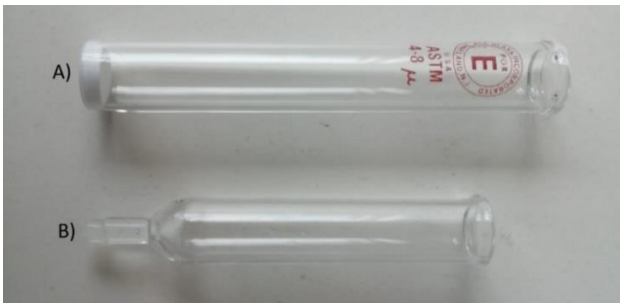

Figure 13: Two tested counter electrode chambers with each its separating porous membrane: A) porous glass frit. B) CoralPor® frit.

2.3. Cyclic voltammetry

In cyclic voltammetry (CV) the redox reactions in a solution are examined. The potential is cycled between two determined potentials at a certain scan rate. The resulting current is measured over the applied potential, resulting in a voltammogram which consists of a negative (reduction) and positive (oxidation) scan (Figure 14). The current peaks observed in a voltammogram come from the oxidation or reduction of a certain species in solution. These peaks show at what potential certain redox reactions occur. When a negative sweep is initiated, a fictive analyte A^+ near the working electrode is reduced to A, the resulting current is determined by the transport of A^+ from the bulk of the solution to the electrode surface. In standard bulk electrolysis the driving force behind the mass transport is diffusion. As the scan continues, the A^+ near the electrode becomes more and more depleted, the diffusion layer grows, which will lower the diffusion rate of A^+ to the electrode surface. On its turn this results in a decrease in the measured current. At the 'switching potential' the scan direction is reversed, now the analyte A will again be oxidized towards A^+ giving an oxidation peak in the measured current.

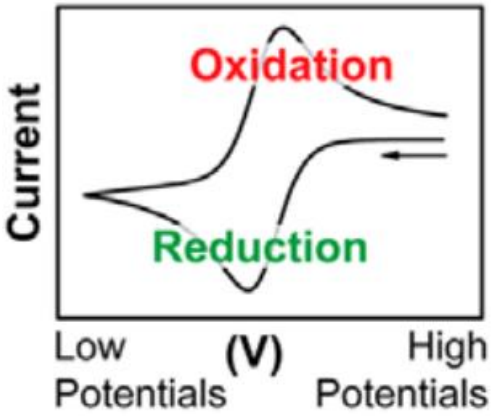

Figure 14: Generalized CV plot according to IUPAC convention.[34]

CV measurements were performed with both types of earlier mentioned potentiostats with the same software Nova 2.1.4. These measurements were done in 10 mL of a Tb^{4+} dilution series to test the quantifiability of Tb^{4+} in solution. The dilution series was made by diluting Tb^{4+} solution with 4 M potassium carbonate solution at pH 14. As a working electrode the earlier mentioned platinum and glassy carbon standard disc electrodes were used, both with the same surface area of 7.1 mm^2.

2.3.1. CV measurements in flow cell

CV measurements were also ran for 0.5 M H_2SO_4 with a Pt working electrode (well-known CV scan) in the flow cell. There were two different types of flow cells available. One where the solution flows radially (radial flow) over the Pt working electrode. The second one where the solution flows across (crossflow) the platinum working electrode. For the cross flow cell there was the possibility of using 2 working electrodes, for the radial flow cell this was not possible. Also the volume differs, for the radial flow cell only 13 µm gaskets were available giving an approximate volume of 0.1 µL, and for the cross flow cell 500 µm and 1000 µm gaskets were used giving an approximate respective volume of 15 µL and 30 µL. The smaller gaskets available for the cross flow cell caused leakage to occur. The flow cells were bought from BASi. To control the flow rates of the solution through the flow cells a PSNE1010 syringe pump from Prosense was used in combination with a syringe of 10 mL from Terumo. For this syringe the flow rate range goes from 16.49 µL/hr up to 36.01 mL/min.

Figure 15: Flow cell experiment setup, with the syringe pump containing the syringe and the assembled radial flow cell.

2.3.2. Linear sweep voltammetry in flow cell

The linear sweep voltammetry is a very similar analysis compared to cyclic voltammetry. Although in this method the potential is swept only once from the set begin potential to the set end potential. Measuring the current response at the working electrode over the linearly increased or decreased potential will show a peak or a plateau at a potential where a certain redox reaction occurs. The scan rates of LSV are much slower compared to those of CV, resulting in a reduced capacitive contribution to the measured current for LSV.

LSV measurements were run in the flow cell to determine the influence of flow on the well-known system of dilute sulfuric acid and a Pt working electrode. The reached plateaus for different applied flow rates were compared to determine the influence of flow.

2.4. UV/VIS spectrometry

In UV/VIS absorbance measurements a range of wavelengths from the UV – visible spectrum range are sent through a solution. Certain wavelengths are absorbed to excite electrons from absorbing species present in solution. In the sensor at the other side of the solution-containing cuvette a reduced intensity for certain wavelengths is observed.

By use of the Lambert-Beer law it should be possible to use the UV/VIS absorbance technique as a quantitative method for the concentration of an absorbing species in solution. In the equation of the Lambert-Beer law A stands for the absorbance, I_0 for the intensity of incident light at certain wavelength, I the transmitted intensity, L the path length through the solution, c the concentration of the absorbing species and ε stands for the molar absorptivity which is specific for a certain absorbing species and as units has $\frac{1}{M} \cdot cm$.

$$A = \log_{10}\left(\frac{I_0}{I}\right) = \varepsilon c L \quad (1)$$

The absorbance measurements were performed at a wavelength range from 230 nm to 1000 nm. The obtained absorbance band from Tb^{4+} complex is a broad band with a peak maximum at about 370 nm caused by a ligand to metal charge transfer (LMCT) of the complexed Tb^{4+}. It was not yet possible to quantify the Tb^{4+}-concentration as the molar absorptivity (ε) is not yet known and couldn't be determined either.

A UV-1800 Shimadzu UV-spectrophotometer which has a resolution of 1 nm, with software UVProbe 2.5 was used for these UV/VIS absorbance experiments. The used cuvette had a path length of 0.1 mm. It was possible to measure the absorbance spectrum while electrolyzing the solution because of the syringe pump of the UV/VIS spectrophotometer. The pump was set to take 2.5 mL out of the cell to measure the absorbance spectrum and afterwards purged the 2.5 mL solution back into the cell.

V. Results and discussion

1. Quantification of Tb^{4+} in solution

The main goal of this thesis was to investigate the electrochemical oxidation of Tb^{3+} in aqueous carbonate solution and optimize the yield of Tb^{4+}. In order to compare the solutions obtained from different oxidation experiments, the produced Tb^{4+} had to be quantified. The possible quantification methods of Tb^{4+} were limited, because of the difficulty in finding a detection method being able to differentiate trivalent and tetravalent terbium.

As mentioned earlier, the oxidation of Tb^{3+} was indicated by a color change from a clear, colorless solution to a dark, red-brown solution. An example of 2 carbonate solutions containing Tb^{3+} are shown in Figure 16, one was oxidized electrochemically and the other wasn't.

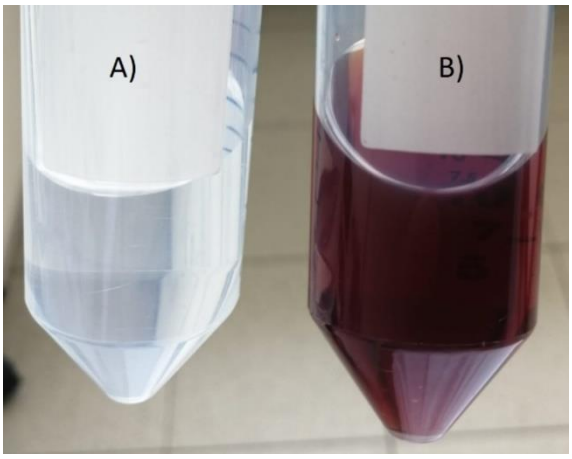

Figure 16: Color change observed for electrochemical oxidation of Tb^{3+} in aqueous carbonate solution. The used concentrations were 4 M K_2CO_3, 70 mM $TbCl_3.6H_2O$ and 75 mM KOH, these concentrations are discussed in the parameter study. A) solution before electrolysis. B) solution after electrolysis.

The color change can be measured by UV/VIS absorbance spectroscopy. The resulting spectra are shown in Figure 17. The formed Tb^{4+}-complex absorbs a wide range of wavelengths in the UV/VIS spectrum, corresponding to a broad band with a maximum at 370 nm. The wavelength of the observed absorbance peak corresponds to the wavelength of the absorbance peak reported by Hobart *et al*.[27] The high intensity of the peak is a result from the ligand-to-metal charge transfer (LMCT). Solvent interaction causes the absorbance band to broaden by allowing a wide range of excitation energies for the electrons.

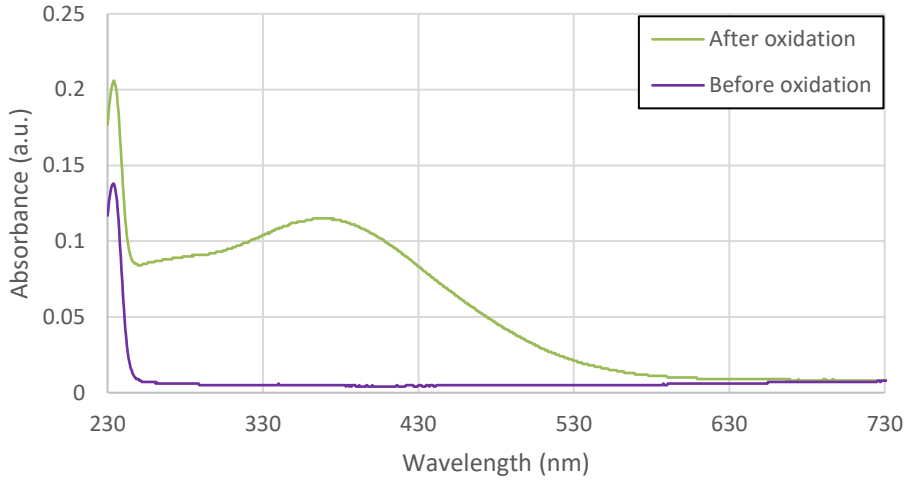

Figure 17: Example of the broad absorbance peak coming from the Tb^{4+}-complex. Measured the UV/VIS absorbance spectra with a cuvette of path length 0.1 mm, before and after electrolysis. The electrolysis was ran for 1 hour by applying +1.3 V vs. Ag/AgCl in 3 M KCl using a Pt working and counter electrode. Cuvette with path length of 0.1 mm was used..

By use of the Lambert-Beer equation (1) it would be possible to quantify the formed Tb^{4+} in solution, however the molar absorptivity (Ɛ) is necessary to calculate the concentration. Aside from two independent estimations made by Hobart *et al*.[27] and Varlashkin *et al*. to be around 1000 $M^{-1}\cdot cm^{-1}$, Ɛ of the carbonate-Tb^{4+} complex is unknown.[17,27]

Nevertheless it is known that the correlation between the concentration and absorbance is linear. This way it is possible to compare results relatively to each other with respect to the concentration. This way of comparing the obtained absorbance values from different solutions, was used by all previously reported research on Tb^{3+} oxidation.

1.1. Quantification using electrochemical methods

The quantification of an occurring redox reaction can be done electrochemically by analyzing the measured current response. By the use of Faraday's electrolysis law, it is possible to quantify the formed ions from electrolysis. Faraday's law dictates that the amount of ions formed in electrolysis is proportional to the amount of current passed.

$$Q = n_e F N \tag{2}$$

Q stands for the total electric charge which is transferred (C), n_e stands for the amount of electrons per mole of reagent, N stands for the amount of moles of formed product and Faraday's constant, $F = 96485 \frac{C}{mol}$. All factors in the Faraday's law are determined beforehand except Q allowing the quantification of the formed species.

However in the studied Tb^{3+} oxidation it was not possible to quantify the formed Tb^{4+}. For the oxidation of Tb^{3+} a potential of +1.3 V vs. Ag/AgCl in 3 M KCl was applied. However at this potential, simultaneously with the Tb^{3+} oxidation, water was being oxidized towards oxygen gas.

$$2H_2O \rightarrow O_2 + 4H^+ + 4e^- \ (+1.23\ \text{V vs. SHE}) \quad (3)$$

Since both oxidation reactions occur at the working electrode, the measured current is a result from both reactions and it is not possible to determine what part of the current is responsible for which reaction. Due to both reactions occurring simultaneously, it was not possible to use Faraday's law to quantify the formed Tb^{4+} on the measured current response from the oxidation reaction.

Therefore, the reduction of Tb^{4+} was investigated with the goal of indirectly quantifying the formed Tb^{4+} on the electrochemical reduction using Faraday's law. For the indirect electrochemical quantification to be possible, Tb^{4+} reduction should be the only reaction occurring at the working electrode for the applied potential. This was investigated by measuring and analyzing the CV scan of Tb^{4+} solutions.

1.2. Cyclic Voltammetry measurements

To examine the occurring electrochemical redox reactions, CV measurements were run with Tb solutions which were electrolyzed to oxidize Tb^{3+} to Tb^{4+}. The total amount of Tb in solution was 70 mM, the reason for this concentration being used is discussed in the next chapter. The CV measurements were performed for both Pt and glassy carbon (GC) working electrodes.

1.2.1. GC working electrodes

In Figure 18 the CV measurements of a blank Tb^{3+} solution and of an oxidized Tb^{3+} solution containing Tb^{4+} are shown. Since the only difference in both solutions is the presence of Tb^{4+} complex in the electrolyzed solution, the differences between both scans should be caused by the Tb^{4+}. The CV scans were measured between -1.5 V and +1 V vs. Ag/AgCl in 3 M KCl, because Hobart *et al*. reported GC electrodes are unstable at higher applied potentials.[27] This also assures the oxidation peak for Tb^{3+} will not be measured as it was determined to be around +1.3 V vs. Ag/AgCl in 3 M KCl.

In the CV of Tb^{4+} solution a reduction peak was observed at -0.3 V vs. Ag/AgCl in 3 M KCl. The occurring reduction peak should be a result from Tb^{4+} reduction, because the CV scan of the solution without Tb^{4+} does not show the reduction peak. This is a first indication of Tb^{4+} reduction occurring at -0.3 V vs. Ag/AgCl in 3 M KCl. To further look into the reduction peak observed in the CV plot a dilution series was made.

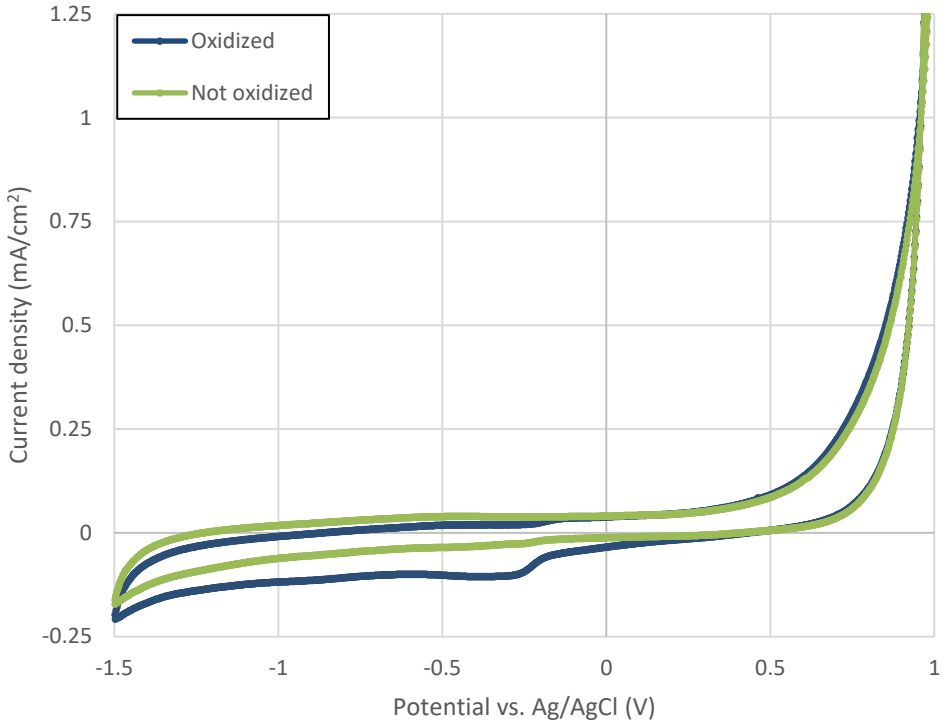

Figure 18: CV measurements with a GC working electrode of a Tb^{4+} solution, which was prepared by oxidizing a Tb^{3+} solution by applying +1.3 V vs. Ag/AgCl for 2 hours and of a Tb^{3+} solution. Measured at scan rate 100 mV/s.

The dilution series was prepared from the oxidized 70 mM Tb solution by diluting with a potassium carbonate solution at pH 14. The different total Tb concentrations (Tb^{3+} and Tb^{4+} combined) in the dilution series are: 70 mM; 35 mM; 20 mM; 15 mM; 10 mM; 7.5 mM and 5 mM. This way the amount of Tb^{4+} in solution was decreased proportionally as much as the total Tb concentration was decreased. CV scans were measured of the dilution series in the same way as done for the measurements reported in Figure 18. The correlation between the measured current at -0.3 V vs. Ag/AgCl and the total Tb concentration are plotted in Figure 19. As the current values are negative, a decreasing trend would be expected for increasing Tb^{4+} concentrations.

From the plot indeed a decreasing trend was observed with a linear correlation ($R^2 > 0.95$). Meaning Tb^{4+} reduction was causing the reduction peak in the CV scan. From these results can be said the reduction of Tb^{4+} is detectable with a GC working electrode. The same experiments were performed with a Pt working electrode to determine whether the Tb^{4+} reduction would still be detectable.

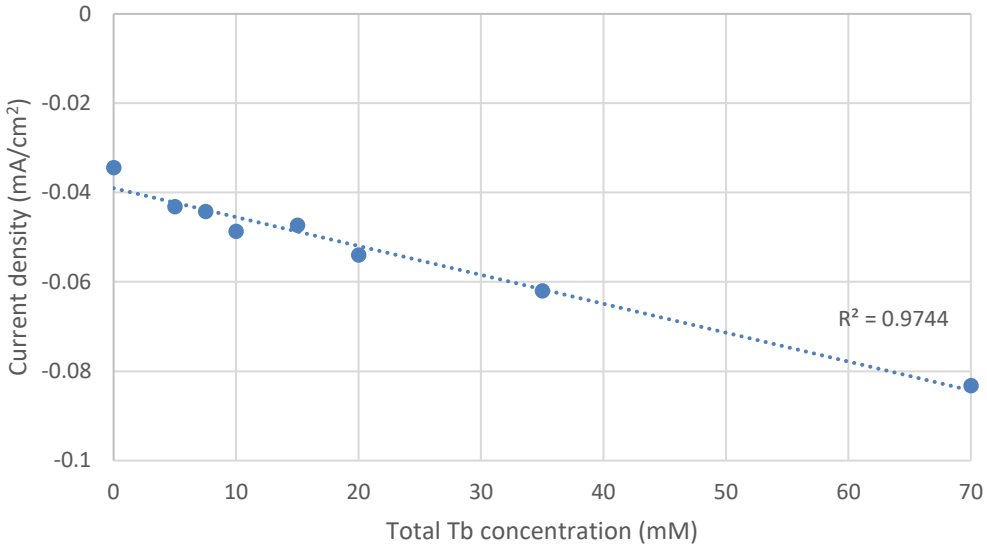

Figure 19: Current values at -0.3 V vs. Ag/AgCl (in 3 M KCl) from the CV measurements with the GC electrode for different total Tb concentrations: 0 mM; 5 mM; 7.5 mM; 10 mM; 15 mM; 20 mM; 35 mM and 70 mM.

1.2.2. Pt working electrode

In a similar way as for the CV measurements with the GC working electrode, the CV scans were measured for the same solutions using the Pt working electrode. The set potential range of the CV was kept the same as for the GC working electrode. Although the lower limit was actually too low, seen by the large decrease in measured current for the potentials below -1 V vs. Ag/AgCl in 3 M KCl. The large current decrease was a result from the hydrogen reduction. In Figure 20 the CV measurements of an oxidized and a blank Tb^{3+} solution are displayed, with on the right a zoomed in version of the peaks of interest.

The CV scans in Figure 20 of both solutions show a reduction peak around -0.4 V and -0.8 V vs. Ag/AgCl in 3 M KCl. The peak at -0.4 V vs. Ag/AgCl in 3 M KCl for the solution containing Tb^{4+} is as pronounced as for the solution containing no Tb^{4+}. For the peak at -0.8 V vs. Ag/AgCl in 3 M KCl the peak is much more pronounced in the solution containing no Tb^{4+}. For both reduction peaks observed in Figure 20 it was indicated the Tb^{4+} reduction cannot be detected while using a Pt working electrode. Because there was no peak measured at more negative currents for the electrolyzed solution compared to the non-electrolyzed solution.

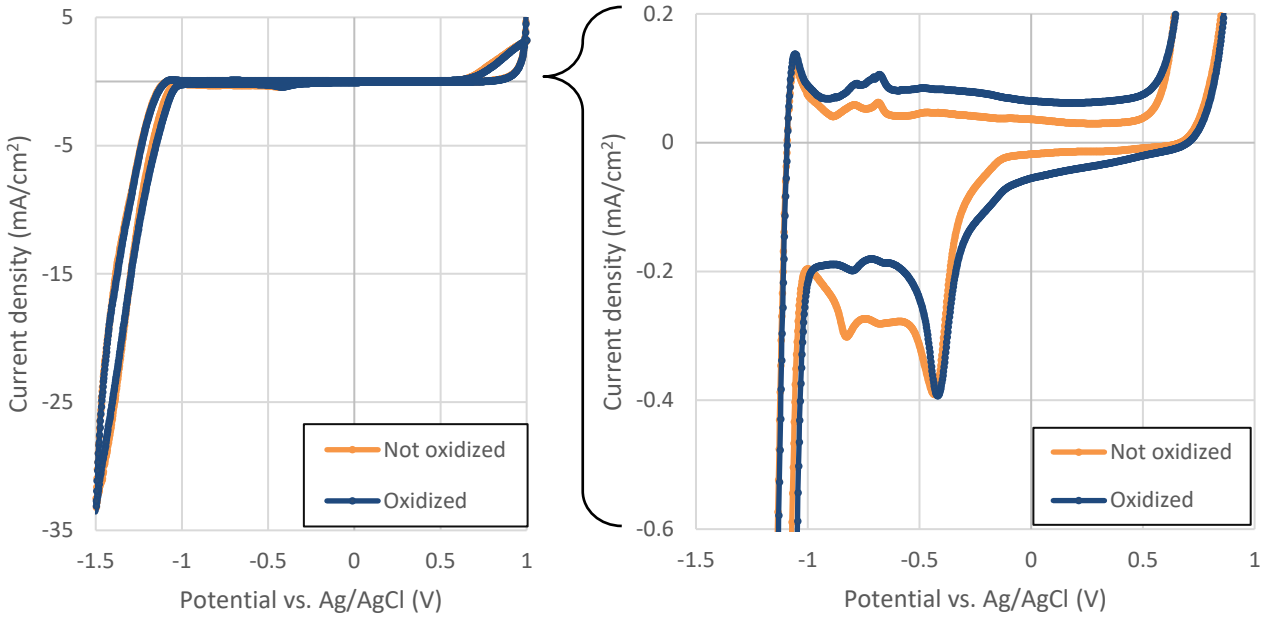

Figure 20: (left) CV plots measured with Pt working electrode of a Tb^{4+} solution, which was prepared by oxidizing a Tb^{3+} solution by applying +1.3 V vs. Ag/AgCl for 2 hours and of a Tb^{3+} solution. (right) same plot as on the left, but zoomed in on lower current densities. Measured at scan rate 100 mV/s.

Although to make sure no rushed conclusions were made as something might have gone wrong in the CV measurement, the same dilution series as CV-scans were measured of using the GC working electrode, were also measured with the Pt working electrode. The obtained currents at the reduction peak of -0.4 V vs. Ag/AgCl in 3 M KCl was shown in Figure 21.

Because the measured data points shown in Figure 21 show no correlation between the measured current at the reduction peak and the amount of Tb^{4+} in solution, it can be concluded no Tb^{4+} reduction was detected using a Pt working electrode. The reduction peak at -0.4 V vs. Ag/AgCl in 3 M KCl might be caused by the back reduction of formed Pt oxides. Since in the oxidation sweep a peak is observed starting from +0.7 V up to +1 V vs. Ag/AgCl in 3 M KCl, which might correspond to the Pt oxides formation.

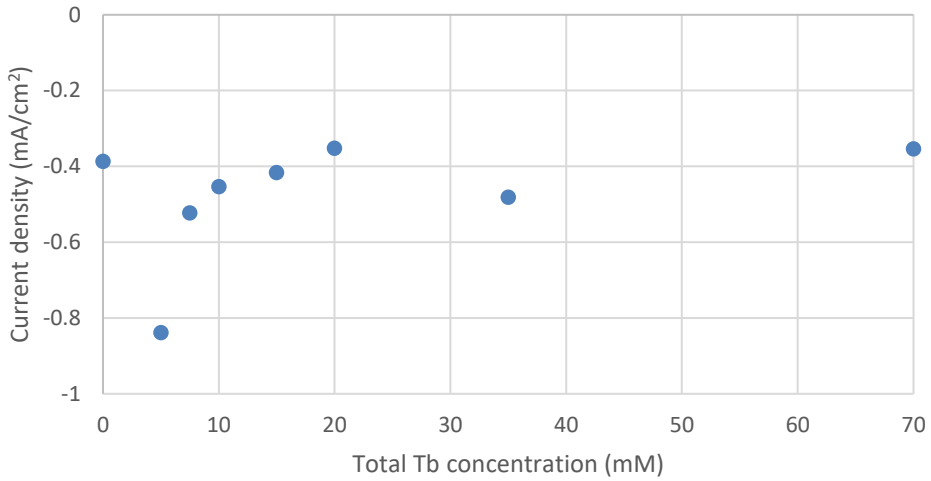

Figure 21: Current values at -0.4 V vs. Ag/AgCl (in 3 M KCl) from the CV measurements with the Pt electrode for different concentrations of Tb in solution: 0 mM; 5 mM; 7.5 mM; 10 mM; 15 mM; 20 mM; 35 mM and 70 mM

For the reduction peak observed at -0.8 V vs. Ag/AgCl in 3 M KCl also no correlation was observed between the measured current at the peak and the amount of Tb^{4+} in solution.

1.3. Tb^{4+} reduction via bulk electrolysis

The CV experiments showed that Tb^{4+} reduction was detected using a carbon working electrode. The reduction of Tb^{4+} was further examined via bulk electrolysis. A reticulated vitreous carbon (RVC) working electrode was used in the bulk electrolysis reduction of Tb^{4+}. From the earlier discussed CV experiments, the potential to reduce Tb^{4+} with the RVC electrode was expected to be -0.3 V vs. Ag/AgCl in 3 M KCl and below.

Various potentials were applied on solutions containing Tb^{4+}, ranging from -0.1 V to -1 V, vs. Ag/AgCl in 3 M KCl, using the RVC working electrode. The reduction of Tb^{4+} was followed by measuring the UV/VIS absorbance values at 370 nm during the electrolysis. When a potential of -0.1 V or -0.2 V vs. Ag/AgCl was applied, no decrease in absorbance values was observed after electrolyzing for over an hour. This indicates no Tb^{4+} reduction occurred at these low potentials. When -0.3 V vs. Ag/AgCl in 3 M KCl was applied a very slight decrease in absorbance values was observed, suggesting a slow Tb^{4+} reduction occurring. Since the decrease was very slow, it was investigated if it would be possible to completely reduce Tb^{4+} by applying -0.3 V vs. Ag/AgCl in 3 M KCl. In Figure 22 the decrease in absorbance at 370 nm is shown as a function of electrolysis time. The large time gap is due to the overnight running of the electrolysis and because the absorbance measurements could not be automized. The absorbance value reaching zero is an indication of complete reduction of Tb^{4+}.

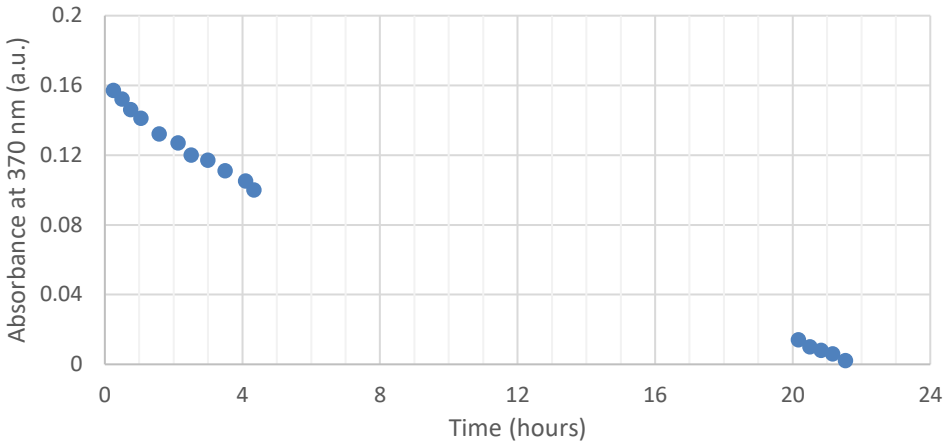

Figure 22: Reduction of Tb^{4+} by applying -0.3 V vs. Ag/AgCl using the RVC working electrode. The absorbance values at 370 nm are shown over time. Cuvette with path length of 0.1 mm was used.

The initial reduction rate was determined from the linear fit on at least 4 absorbance values measured in the first hour of reduction. The slopes in the decrease in absorbance values over time were shown in Figure 23. For -0.4 V and -0.6 V vs. Ag/AgCl in 3 M KCl, the applied potentials were off, for this reason these potentials were not included. The lowest potentials of -0.9 V and -1 V vs. Ag/AgCl in 3 M KCl correspond to the fastest reduction rates, which confirms the expectations.

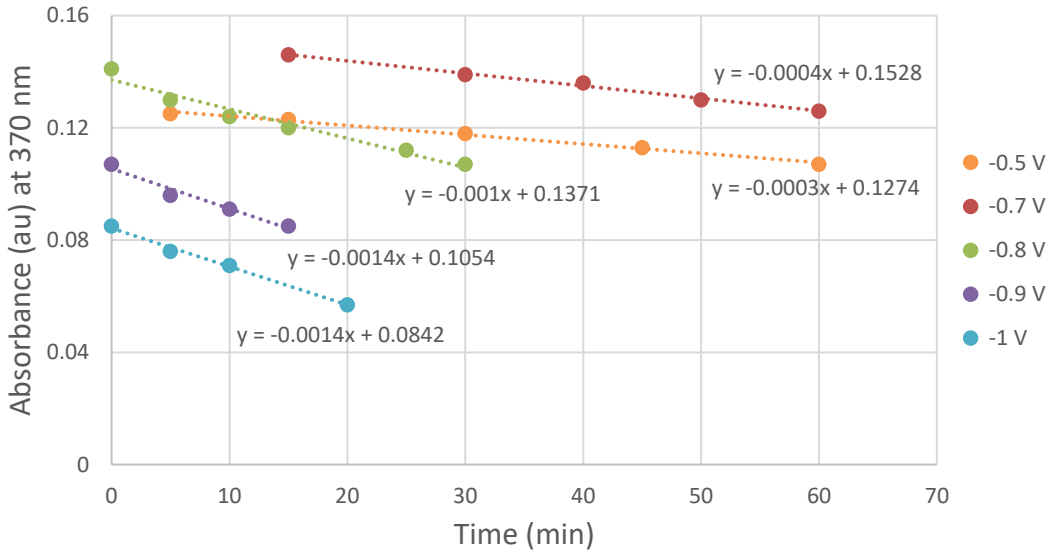

Applied potential (V)	-0.3	-0.5	-0.7	-0.8	-0.9	-1
Reduction rate (a.u./min)	-0.0002	-0.0003	-0.0004	-0.0010	-0.0014	-0.0014

Figure 23: Reduction rates for different applied potentials, obtained from the fitted linear trend in decrease in absorbance over time while electrolyzing. For all linear fits of the decreasing trend a R^2 value of at least 0.95 was obtained. Cuvette with path length of 0.1 mm was used.

1.4. Calculations for electrochemical reduction of Tb^{4+}

The experiment above of complete Tb^{4+} reduction at a potential of -0.3 V vs. Ag/AgCl in 3 M KCl, was used in the electrochemical quantification attempt. The measured current response from the complete reduction is shown in Figure 24. A remarkable observation from the current response is the fact the measured current didn't go to zero by the time the absorbance value at 370 nm reached zero, this might indicate there still is a reduction occurring. Although due to time limitation the overnight electrolysis was not repeated. To obtain the total amount of electric charge transferred Q, the surface area between the curve and the x-axis was measured resulting in 34.17 C.

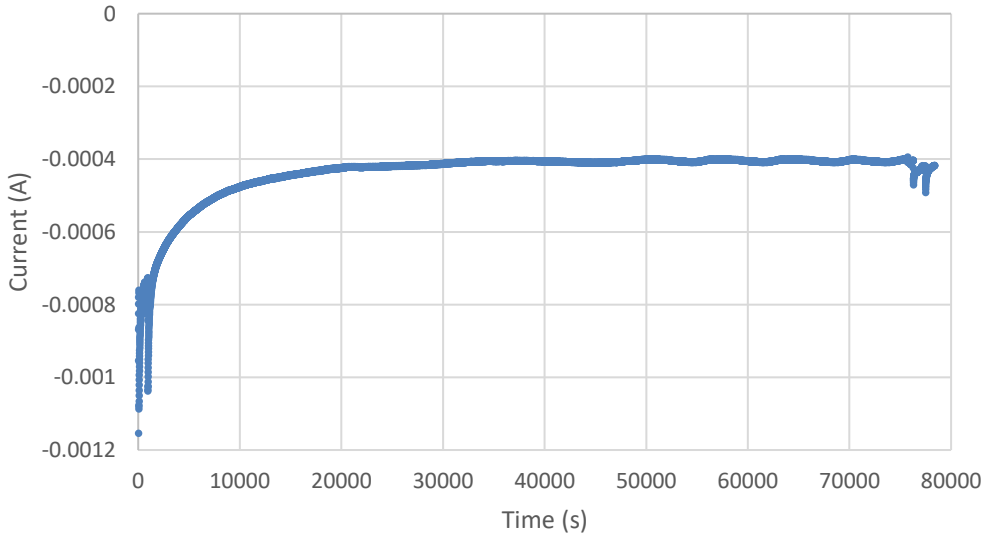

Figure 24: Measured current response for the complete Tb^{4+} reduction at -0.3 V vs. Ag/AgCl.

In the following equation the amount of formed Tb^{4+} was calculated using Faraday's law. The amount of Tb^{4+} formed was determined to be 0.35 mmol. Since the reduction experiment was performed in 20 mL this gave a concentration of 17.7 mM Tb^{4+} in solution.

$$N = \frac{Q}{n_e F} = \frac{34.17\ A{\cdot}s}{96485\ \frac{C}{mol}} = 3.54 \cdot 10^{-4}\ mol \quad (4)$$

$$c = \frac{3.54{\cdot}10^{-4}\ mol}{0.02\ L} = 17.7 \cdot 10^{-3}\ M \quad (5)$$

The concentration determined electrochemically, was compared with the concentration determined with the Lambert-Beer equation, using an estimated value for the molar absorptivity determined by Varlashkin *et al*. and Hobart *et al*. to be about 1000 $M{\cdot}cm^{-1}$.[17,27] The absorbance value at 370 nm of Tb^{4+} solution before reduction was 0.152 a.u.. In the equation below, the concentration of Tb^{4+} in solution before reduction was determined with the Lambert-

Beer equation using the estimated molar absorptivity. The path length of the used cuvette was 10^{-2} cm. The determined concentration is 15.2 mM.

$$c = \frac{A}{\varepsilon L} = \frac{0.152 \text{ a.u.}}{1000 \text{ M}^{-1}\cdot\text{cm}^{-1}\cdot 10^{-2}\text{cm}} = 1.52 \cdot 10^{-2} \text{ M} \quad (6)$$

The total Tb concentration in solution was known to be 70 mM, although the amount of Tb in tetravalent state was unknown. From these results it was found that over 20% of Tb in solution was in tetravalent state. The complete electrochemical reduction of Tb^{4+} was possible, and could be used to determine the Tb^{4+} concentration, because the electrochemically determined concentration was close to the estimated concentration via UV/VIS absorbance spectroscopy. Although it has to be taken into account that for the measurement used for the electrochemical quantification, the measured current didn't approach to zero as would be expected.

Due to time limitation the electrochemical quantification of Tb^{4+} in aqueous carbonate solution was not further investigated. However from these results and observations, suggestions were given for future research on electrochemical Tb^{4+} quantification. The fact the measured current didn't approach to zero, suggests there still was a reduction occurring. To make sure the measured current doesn't approach to zero, similar reduction experiments could be performed. The electrochemical reduction should be performed on a dilution series of Tb^{4+} in aqueous carbonate solution. Subsequently determine the molar absorptivity using the Lambert-Beer equation with the obtained concentrations and the measured absorbance values of the dilution series before reduction.

2. Parameter study for bulk electrolysis

In the following chapter a detailed parameter study on Tb^{3+} oxidation in bulk electrolysis was investigated. The concentration ranges of $TbCl_3.6H_2O$ and K_2CO_3 were determined based on previous results from the ongoing PhD project of Meryem Arman at SCK CEN. The influence of deviating the pH from 14 was also discussed. The temperature of the solution during electrolysis was also varied to investigate the influence. To determine the most efficient conditions for each parameter the absorbance values at 370 nm of the obtained solutions, were compared relatively to each other. The solutions were not quantified exactly because the method discussed above only is an approximation and more experiments should be ran to verify the obtained results.

2.1. Optimization of salt concentrations

The concentrations of $TbCl_3\cdot 6H_2O$ and K_2CO_3 were investigated. The Tb-concentration were varied between 40 mM and 100 mM and the tested K_2CO_3 concentrations were 3 M; 4 M and 5 M. These ranges were determined by previous research. Concentrations below 40 mM and

3 M for Tb and K_2CO_3 respectively, were reported to give no indication of formed Tb^{4+} in solution. For concentrations exceeding the upper limits formation of precipitate was reported. The concentration experiments were conducted in the small volume setup of 5 mL for 2 hours of bulk electrolysis. For all reported concentration combinations the broad absorbance band with a maximum at 370 nm, of which an example was shown in Figure 17 was observed. In Figure 25 the absorbance values at 370 nm are shown for different concentrations of Tb and K_2CO_3, each concentration combination was performed only once. The error bars indicated in the plot are set at a constant 0.01 a.u. which is an estimated uncertainty, taking into account the possible different interelectrode distances and slightly deviating concentrations for different electrochemical experiments.

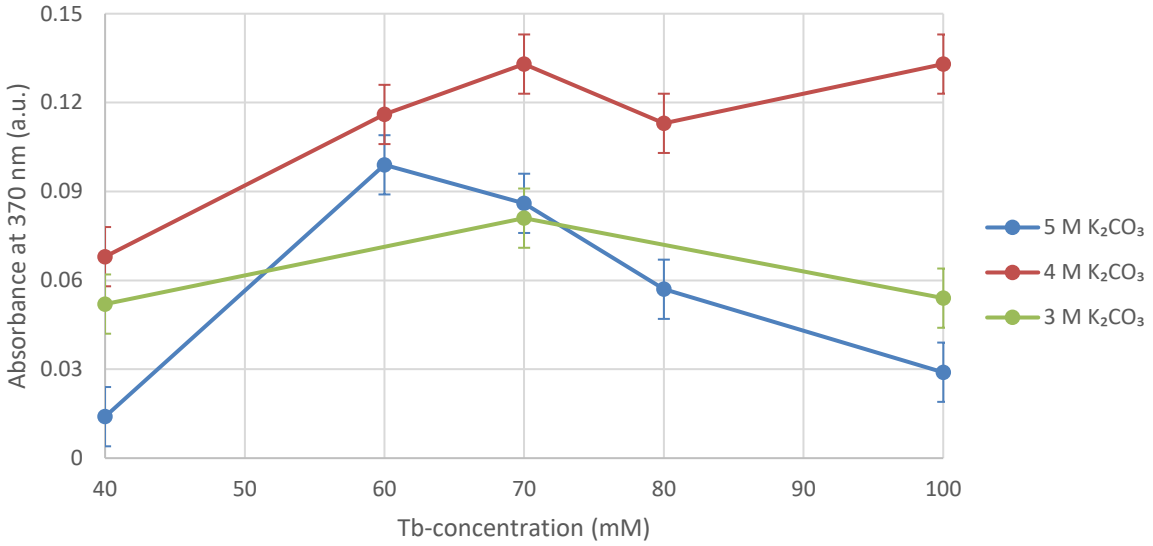

Figure 25: Concentration influence on absorbance. The solutions were oxidized by applying +1.3 V vs. Ag/AgCl in 3 M KCl, for 2 hours using a Pt working and counter electrode in small volume setup of 5 mL. Cuvette with path length of 0.1 mm was used.

By comparing the absorbance values measured at 370 nm relatively to each other, it was found that after 2 hours of electrolysis the oxidation of Tb^{3+} conducted in 4 M K_2CO_3 solution, obtained the highest Tb^{4+} concentration. At 4 M K_2CO_3 the amount of carbonate anions was more suitable for efficient formation of stable Tb^{4+} complexes, compared to solutions containing 3 M and 5 M K_2CO_3 in solution. This can be explained by the formation of a stable Tb^{4+} complex which consist of both carbonate and hydroxide anions, confirming the reasoning of Varlashkin *et al*. mentioning a too high concentration of K_2CO_3 inhibits the formation of the stable hydroxo/carbonate Tb^{4+} complex.[17] Therefore, for the following experiments a K_2CO_3 concentration of 4 M was used.

When looking further into the different concentrations of Tb for 4 M K_2CO_3, it was found that 40 mM, 60 mM and 70 mM Tb gave increasing absorbance values for increasing Tb concentrations after 2 hours of oxidation at +1.3 V vs. Ag/AgCl in 3 M KCl. This result indeed corresponds to what was expected, higher absorbance values indicate a higher amount of Tb^{4+} ions in solution. The absorbance values after 2 hours of electrolysis for concentrations of 70 mM Tb and larger obtained similar values, indicating a plateau was reached.

When analyzing the results obtained for different Tb concentrations in 3 M K_2CO_3 and 5 M K_2CO_3, a different trend was observed. The absorbance values seem to reach a maximum at 60 or 70 mM. This possibly could be caused by an ideal ratio of Tb versus carbonate anions in solution. Anyhow when combining the results of all 3 carbonate concentrations, 60 or 70 mM was observed to be the most efficient Tb concentration. Because in 4 M K_2CO_3, 70 mM Tb was found to be most efficient, the following experiments were conducted with a solution consisting of 4 M K_2CO_3 and 70 mM $TbCl_3 \cdot 6H_2O$.

2.2. pH dependency

Hobart *et al*. reported the pH of the carbonate Tb solution had to be adjusted to 14 by adding KOH for stability of Tb^{4+} complexes in the solution.[27] In the following section it was investigated if Tb^{3+} oxidation would still occur for pH values deviating from 14. Three solutions at different pH were prepared, by adding a various amount of KOH. When no KOH was added to the solution, a pH of 13.1 was measured due to the potassium carbonate. For the next solution 30 mM KOH was added to obtain a pH of 13.5, as a third solution the pH was adjusted to 14 by adding 75 mM KOH. When adding more KOH to the solution an insoluble precipitate was formed, expected to be a terbium-hydroxide compound.

When the three different solutions were electrolyzed, color change was observed for the solution at pH 14. For the solutions at pH 13.1 and pH 13.5 no coloration was observed. The absorbance spectra of all three solutions were measured after electrolyzing (Figure 26), giving no indication of Tb^{4+} in solutions of pH 13.1 and pH 13.5. For Tb^{3+} oxidation to occur, a pH of 14 was determined to be necessary. A possible explanation might be, to form the stable complex consisting of both hydroxide and carbonate anions, a very high concentration of hydroxide anions is necessary to make enough hydroxide anions able to coordinate to the formed Tb^{4+}. For the following experiments KOH was added to obtain a concentration of 75 mM to maintain the same concentrations over different experiments, occasionally the pH was measured to make sure it was 14.

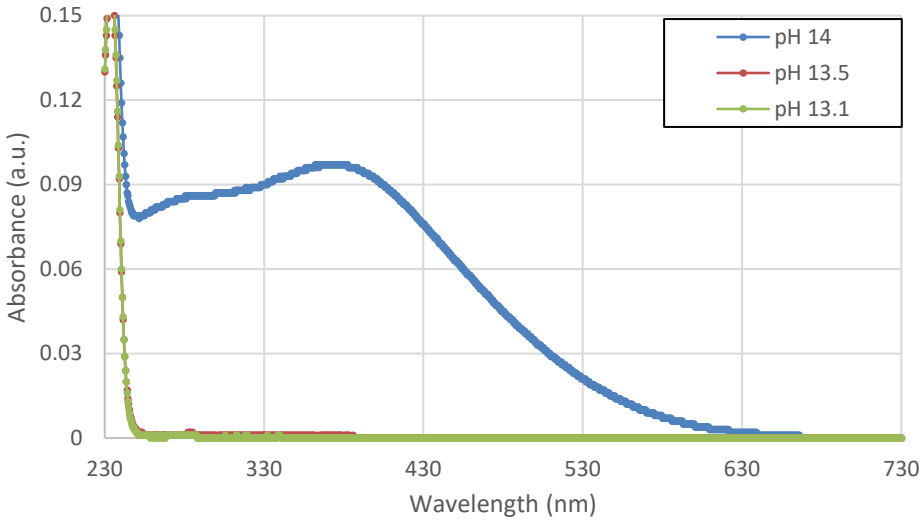

Figure 26: Tb^{3+} solutions, one at pH 13.1, one at pH 13.5 and one at pH 14 were electrolyzed by applying +1.3 V vs. Ag/AgCl in 3 M KCl for 1 hour. The three absorbance curves are shown, with the curves for pH 13.1 and 13.5 overlapping. Cuvette with path length of 0.1 mm was used.

2.3. Temperature dependency

The temperature was varied between 5°C and 40°C. This range was chosen to maintain the stability of the reference electrode. For all different temperatures at least three solutions were electrolyzed for 2 hours at +1.3 V vs. Ag/AgCl in 3 M KCl, to use the average absorbance values at 370 nm in the comparison of solutions at various temperatures. During the electrolysis every 15 minutes an absorbance measurement was done to follow the Tb^{3+} oxidation over time.

As an initial result, Tb^{3+} oxidation was found to be possible in the whole temperature range of 5°C up to 40°C. In Figure 27, the average absorbance value of 3 repetitions measured at the same temperature and electrolysis time are shown for the various temperatures. There is an increasing trend of absorbance over time observed for all temperatures of solution. Since the plots were going towards a plateau, the oxidation rate was determined to decrease over time, meaning the Tb^{3+} in solution was getting depleted. Although in the last 15 minutes interval of oxidation there was still an increase in Tb^{4+}. This suggests the maximal amount of formed Tb^{4+} was not yet reached for any of the 5 different temperatures after 2 hours of electrolysis at +1.3 V vs. Ag/AgCl in 3 M KCl.

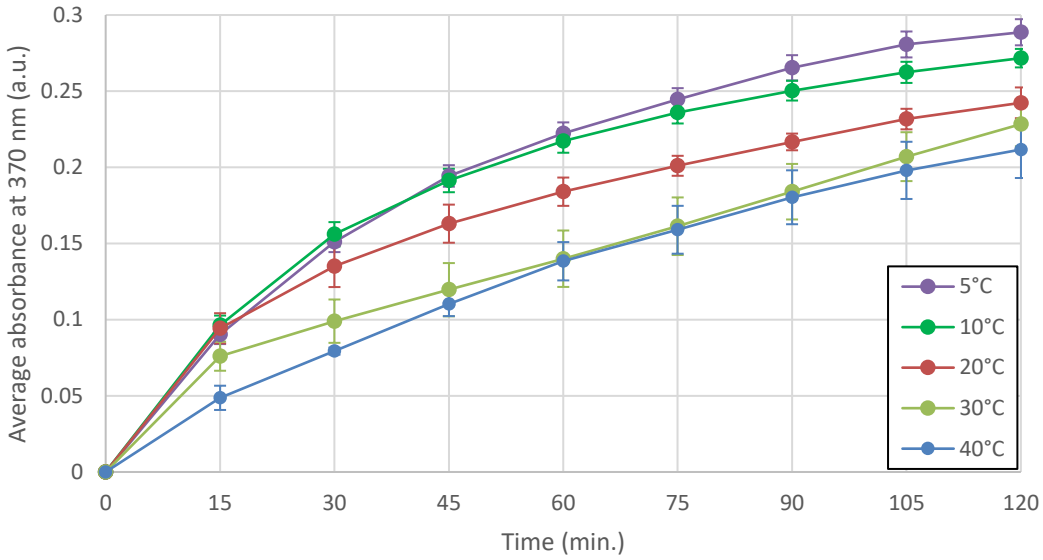

Figure 27: Average absorbance maxima for 3 solutions at 5°C, 10°C, 20°C, 30°C or 40°C of 4 M K_2CO_3, 75 mM KOH and 70 mM $TbCl_3.6H_2O$ after 2 hours of applying +1.3 V vs. Ag/AgCl in 3 M KCl. Cuvette with path length of 0.1 mm was used.

In Figure 28 a plot is shown of the average absorbance values at 370 nm after 2 hours of electrolysis, giving the relation between the temperature and Tb^{3+} oxidation of 2 hours. A decreasing trend in absorbance values for increasing temperature of solution was recognized after 2 hours of oxidation. This corresponds to the most Tb^{4+} formed in solutions at 5°C compared to the solutions at higher temperatures. These results are similar to what Xiaojing *et al*. had observed for Tb^{3+} oxidation in tetrametaphosphate solution.[29] For their system they suggested this might be caused by the increased rate of Tb^{4+} reduction at higher temperatures. However they mention their formed Tb^{4+} complex isn't stable over time, supporting this suggestion. The increased reduction rate at higher temperatures was not the case for the carbonate complexes, because it was determined to be stable up to several weeks.

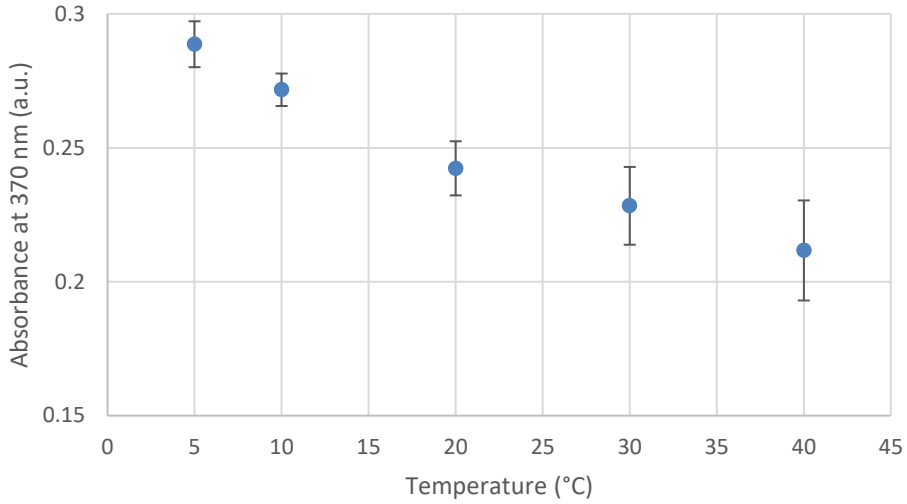

Figure 28: Absorbance values at 370 nm measured with a cuvette of path length 0.1 mm, after oxidizing for 2 hours at +1.3 V vs. Ag/AgCl in 3 M KCl at 5°C, 10°C, 20°C, 30°C and 40°C.

Another observation that was made clear in Figure 28 is the increasing size of the standard error bars for increasing temperature of solution. This indicates the electrochemical oxidation at higher temperatures is not as reproducible compared to the reproducibility of solutions at lower temperatures.

3. Tb^{3+} oxidation in different electrolytic celltypes

For the previous electrochemical experiments, bulk electrolytic cells were used where the working and counter electrode were both in the bulk solution without any separation in between and the mass transport in the cell was determined purely by diffusion. In the following section, experiments are described where the system deviated in a certain way from the standard bulk electrolysis setup.

3.1. Flow cell

As a first alternative electrolytic cell, the flow cell was examined. In this type of cell the solution is flowed at a constant flow rate through the cell, while passing the working and counter electrode. Similarly as in bulk the applied potential for Tb^{3+} oxidation was +1.3 V vs. Ag/AgCl in 3 M KCl. Two different types of flow cells were used, one where the solution flows radially over the working electrode, referred to as the radial flow cell and another one where the solution flows across the working electrode, referred to as the cross flow cell.

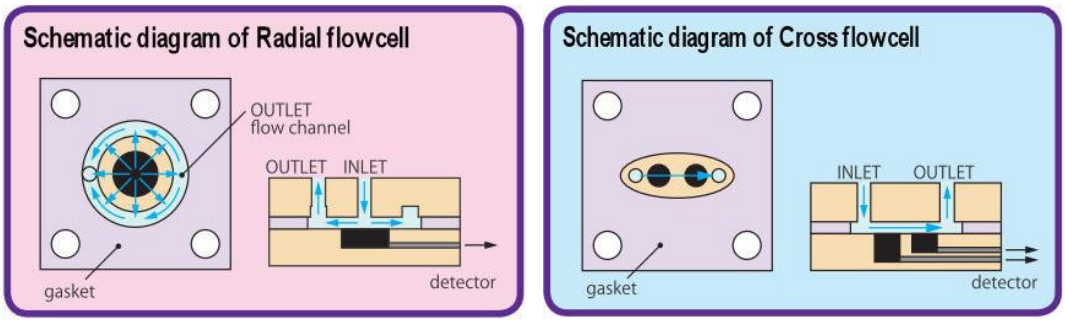

Figure 29: Schematic presentation of on the left the radial flow cell and on the right the cross flow cell. Pictures copied from ALS-Japan.com[35]

For the bulk electrolytic cell diffusion is responsible solely for mass transfer of Tb^{3+} to reach the working electrode. In the flow cell mass transfer of Tb^{3+} is simultaneously regulated mechanically by the syringe pump, of which the pump speed can be set very precise and a faster mass transport can be achieved compared to diffusion.

The flow cell volumes were determined by the cell gaskets, for the radial flow cell there were 4 gaskets available with a thickness of 13 µm, it was possible to stack 2 of them, but using 3 or 4 resulted in leakage of the cell. For the cross flow cell there were 4 different sizes available: 50 µm, 100 µm, 500 µm and 1000 µm, although for the 2 smallest gaskets also leakage occurred which wasn't possible to prevent. Based on these, the volumes were approximately 0.1 µL for 2 gaskets in the radial flow cell and 15 µL or 30 µL for the 500 µm and 1000 µm gaskets of the cross flow cell respectively.

From the cell volumes another reason was found why the flow cell was expected to be more efficiently compared to bulk electrolysis. The larger working electrode-surface/volume of solution. The larger this ratio, the faster the present Tb^{3+} could be oxidized completely. The surface area of the Pt gauze used for bulk electrolysis is 70 cm^2 for a solution of 50 mL, giving a ratio of 1.4 cm^2/mL. Where the flow cell used a Pt electrode of $7 \cdot 10^{-2}$ cm^2 for a volume of 0.1 µL for the radial flow cell and 15 µl or 30 µL for the cross flow cell, giving a ratio of respectively 700 cm^2/mL and 4.7 cm^2/mL or 2.4 cm^2/mL. Another benefit when reflecting back at the bigger picture of ^{161}Tb production, would be the possibility of in-line oxidation, allowing the automation of the production.

3.1.1. Parameter study on a well-known system

To test the influence of different flow parameters on electrochemical reactions, the influence of flow on the CV of 0.5 M H_2SO_4 measured with a Pt working electrode, was investigated. In Figure 30 the typical CV scan using the Pt working electrode in the aforementioned solution of conducting agent, sulfuric acid, is shown. In Figure 30, the occurring reactions corresponding to the observed peaks where included. In the negative potential region H^+ is getting reduced

to adsorbed hydrogen and back oxidized towards H^+ upon reversing the scan direction. In the positive potential region Pt-oxides are formed, which are reduced back when the sweep direction is reversed. The double layer region consists of a layer of anions/ cations next to the electrode surface and a second layer of cations/ anions respectively. The ions are loosely associated with the electrode surface, moving under influence of the electric attraction.

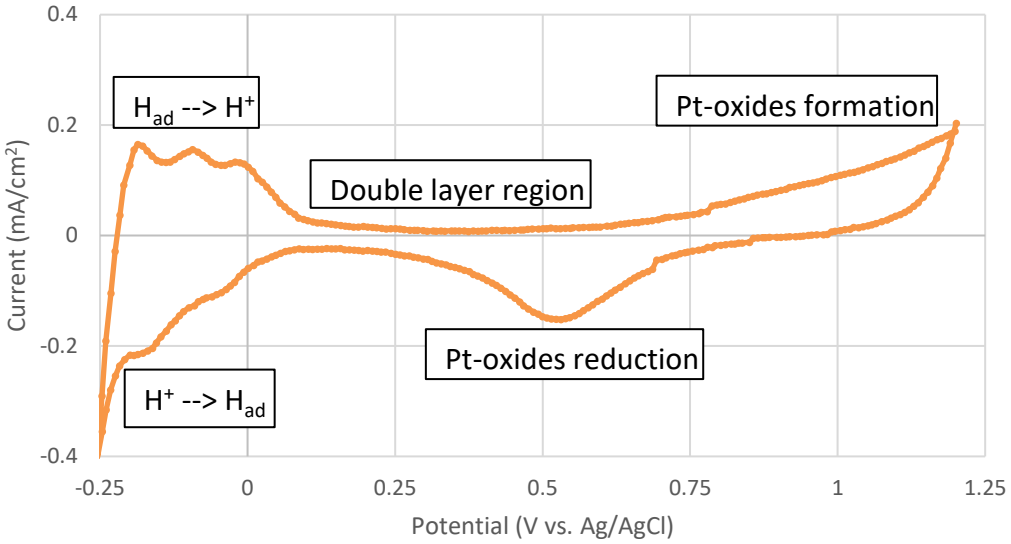

Figure 30: CV scan of 0.5 M H_2SO_4 with a Pt working electrode, measured in a bulk cell with scan rate of 100 mV/s and a Pt working electrode surface of 0.071 cm^2 and 0 µL/min flow.

The different parameters which were varied are the following: flow rate, cell volume and the counter electrode connection site (Figure 31). The flow rate was determined by the syringe pump and has been varied in a range from 1 µL/min up to 1 mL/min. The cell volume was determined by the cell gaskets, as mentioned before. For the radial flow cell there were two possible connections for the counter electrode shown in Figure 31, either the metal block or the metal outlet tube.

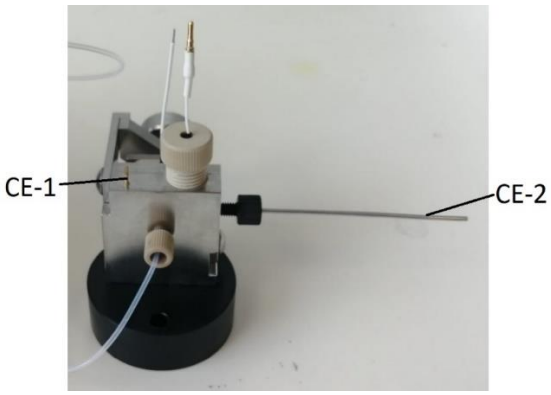

Figure 31: Radial flow cell with 2 possible connection sites indicated for the counter electrode. CE-1: the metal block of the cell and CE-2: the metal outlet

For the CV scan of dilute sulfuric acid without flow, the scan rate was varied to determine up to which scan rate the obtained plots would be noise-free. In figure 32 the CV scans are shown, measured at different scan rates. It was found that scan rates of 150 mV/s, 250 mV/s and 500 mV/s gave too much noise and the scans for 80 mV/s and 100 mV/s gave a smooth plot. The scan rate was kept fast enough to minimize measurement time. Therefore, a scan rate of 100 mV/s was used for all the following CV measurements.

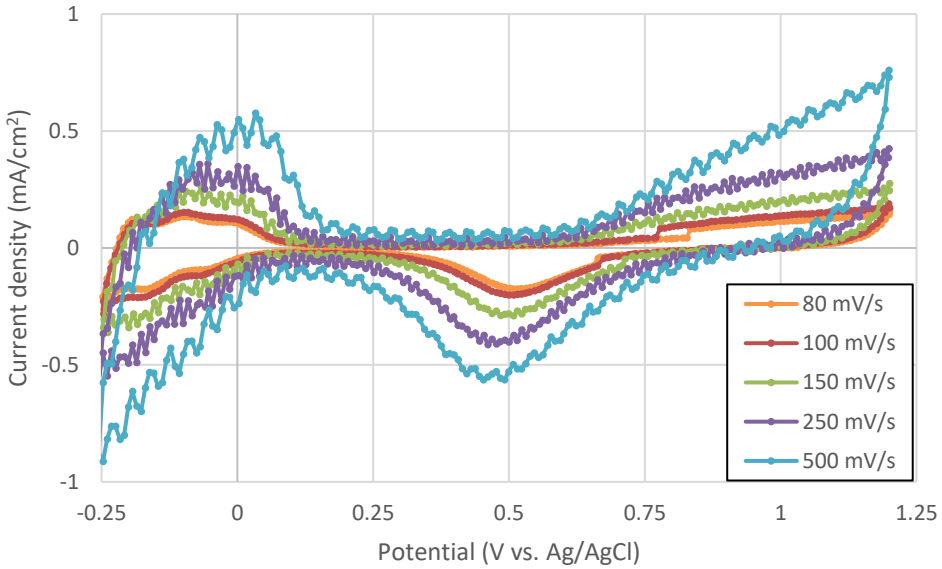

Figure 32: CV measurements for 0.5 M H_2SO_4 measured with Pt working electrode at different scan rates: 80 mV/s, 100 mV/s, 150 mV/s, 250 mV/s and 500 mV/s. All measured at 0 µL/min flow rate.

To examine the influence of the counter electrode connection site on the measured CV plots, scans were measured for different flow rates with the counter electrode connected at the outlet for one set of experiments and with the counter electrode connected to the bulk of the cell for another set of experiments. It was found that the counter electrode connection site didn't influence the measurement. For the following measurements performed in the radial flow cell the counter electrode was attached on the outlet of the cell, because the attachment to the bulk of the cell was no option for the cross flow cell. This way they both have a similar counter electrode placement.

The influence of the cell volume and the flow rate on the system were examined simultaneously. Because both parameters determine the residence time of the solution in the cell, the residence time decreases for faster flow rates and smaller cell volumes. For the cell volume there were three options compared, the radial flow cell had an approximate volume of $1 \cdot 10^{-4}$ mL and the cross flow cell had an approximate volume of $1.5 \cdot 10^{-2}$ ml or $3 \cdot 10^{-2}$ mL for the 500 µm and the 1000 µm gaskets respectively. The flow rate was varied in a range from 1

µL/min up to 1 mL/min. In Table 7 the ranges of the flow rate were converted to ranges of residence time for the different cell volumes.

Table 7: The ranges of flow rate converted to ranges of residence time for the 3 different cell volumes (0.1 µL; 15 µL and 30 µL).

Different cell volumes	Residence time for 1 mL/min flow (s)	Residence time for 1 µL/min flow (s)
Radial flow cell (0.1 µL)	0.006	6
Cross flow cell (15 µL)	0.9	900
Cross flow cell (30 µL)	1.8	1800

In Figure 33 an example of the CV scan measured while solution is flowed through with a low residence time the radial flow cell is shown together with a CV scan where the solution was stationary. The influence of the flow is observed in the deformation of the hydrogen region of the plot. The hydrogen region was shifted to more negative potentials and the positive potential region remained unaffected.

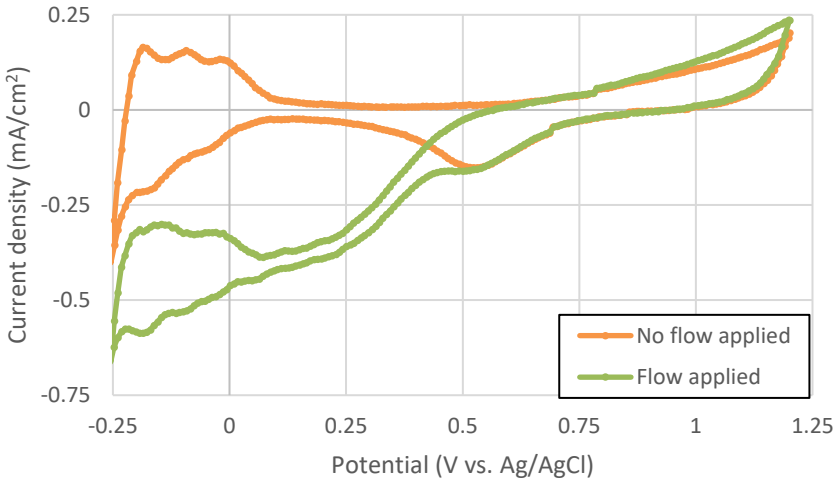

Figure 33: CV scans for 0.5 M H_2SO_4 with a Pt working electrode in the radial flow cell. Plotting 0 µL/min and 50 µL/min, corresponding to 0.12 seconds residence time. Measured with scan rate of 100 mV/s.

In Figure 34 the measured current at +0.1 V vs. Ag/AgCl in 3 M KCl is shown as a function of residence time, this way the deformation of the CV plot was indicated. In the displayed scatter plot, data points obtained with both the radial and the cross flow cell were included. Due to the big difference in volume and with it the order of magnitude, the residence time on the x-axis is shown in a logarithmic scale.

From figure 34 it was confirmed that for longer residence times the obtained CV plots were more similar to the typical CV plot obtained in the bulk cell, displayed in Figure 30. For

residence times longer than 1 s, the influence of the flow was negligible. While running a CV measurement, the occurring reactions all happen in the narrow layer of solution near the electrode surface. For fast flow rates it was expected the ion layer near the electrode surface would be agitated too much, leading to the CV scan being more influenced for the lower residence times.

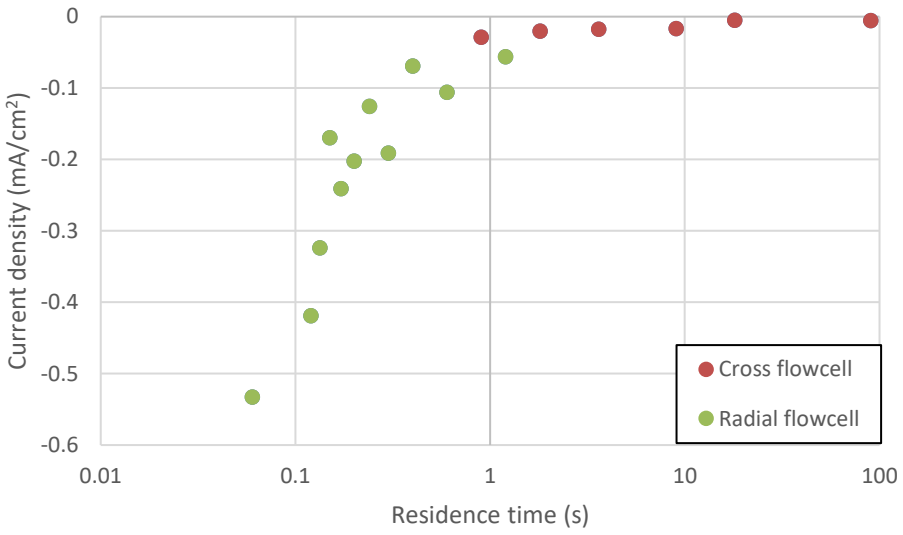

Figure 34: Current density values at +0.1 V vs. Ag/AgCl of the reduction sweep from the CV scan are shown for different residence times. The data points are from both the radial and cross flow cell.

3.1.2. Oxygen reduction reaction (ORR)

In the following section the influence of the flow parameters were investigated on the oxygen reduction reaction (ORR) in dilute sulfuric acid by saturating the solution with oxygen gas.

$$O_2 + 4H^+ + 4e^- \rightarrow 2H_2O \quad (7)$$

To saturate the dilute sulfuric acid with oxygen, the solution was purged for at least 30 minutes with air. A CV scan was measured to determine the potential where the ORR takes place. From the CV scan shown in Figure 35 the ORR was shown to occur at +0.25 V vs. Ag/AgCl in 3 M KCl, because this reduction peak was not observed for the earlier discussed CV scans where the solution was not saturated with oxygen.

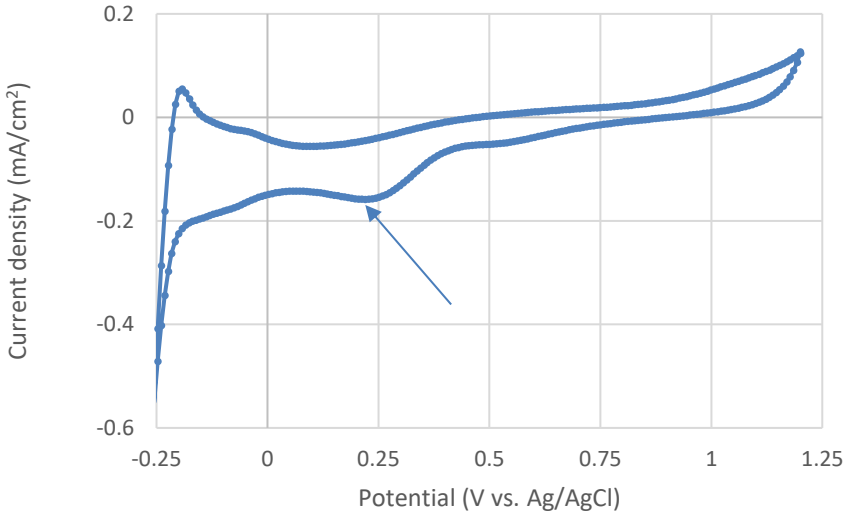

Figure 35: CV measurement of 0.5 M H_2SO_4 saturated with oxygen. The oxygen reduction peak is indicated in the figure. The scan was measured at scan rate 100 mV/s and 0 µL/min flow rate.

From the obtained result in Figure 35, the potential range of the LSV was determined to be ran between 0 V and +1.1 V vs. Ag/AgCl in 3 M KCl. The LSV measurements were performed at different flow rates, this way the influence of the flow on the ORR was determined. In figure 36 LSV scans were shown of some residence times as an example. It was seen that for the longer residence times above 0.6 s a clear plateau was reached in the LSV scan for potentials below +0.2 V vs. Ag/AgCl. For the lowest residence times below 0.6 s, the plateau in the LSV scans start decreasing and disappear for lower residence times. On the right in figure 36, the correlation is shown between the current measured at the plateau and the residence time. From the correlation plot it was observed the residence time shorter than 1 s showed the most pronounced influence from the flow. The decrease in current and deformation of the plateau is an indication of a too short residence time. As a conclusion, the results are in parallel with the cyclic voltammetry. When the residence time was decreased below 1 s the system was influenced from the applied flow, because the electrolytic reactions no longer had sufficient time to occur. This conclusion was based on results of both the LSV and CV experiments.

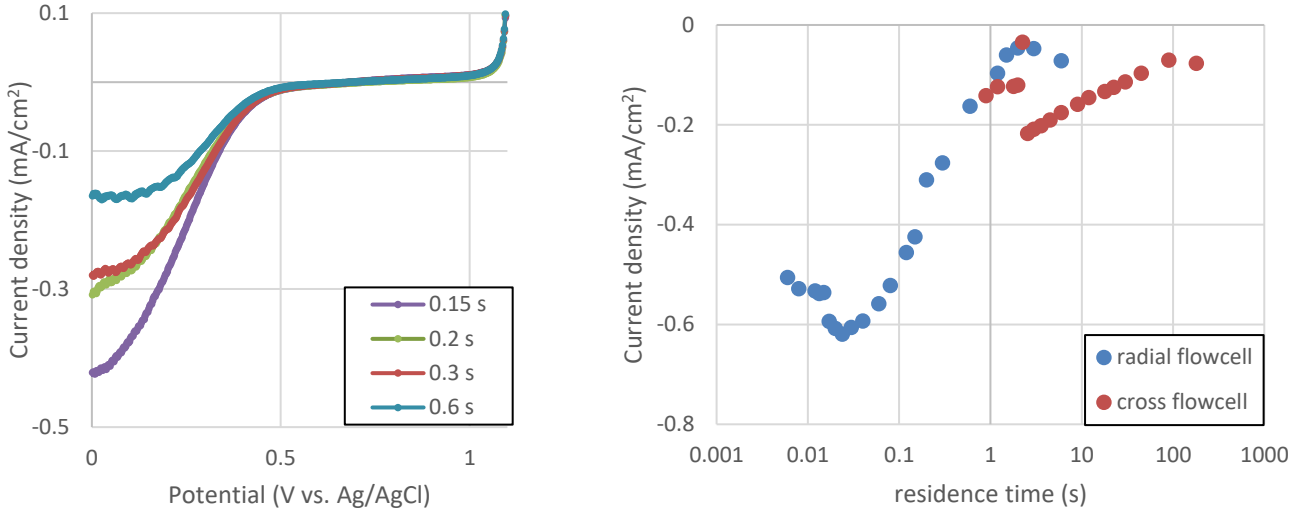

Figure 36: LSV scans for different residence times (0.15 s; 0.2 s; 0.3 s and 0.6 s).

3.1.3. Oxidation of Tb^{3+} in flow cell

From the flow cell experiments discussed above, the least influence of flow on the investigated systems was found for residence times longer than 1 s. Due to the larger volume of the cross flow cell the residence times were all larger than 1 s for all applied flow rates in this cell. The residence time of 1 s was found to be a limit, where for shorter residence times the influence of the flow on the previously investigated system was observed to be more pronounced.

At previous Tb^{3+} oxidations in bulk, there was a simultaneous gas formation at the working electrode of oxygen gas. When oxidizing Tb^{3+} in the flow cell, the formation of oxygen gas was expected to be a possible problem, therefore the gas formation was followed closely. For too much gas formation the cell might be expected to clog, preventing the application of the correct potential.

The following parameters were varied for the Tb^{3+} oxidation attempts in the flow cell. The residence time determined to give the least influence when kept above 1 s, although it was also attempted at lower residence time as a shorter residence time was expected to reduce the total volume of gas in the flow cell by purging out the gas faster. The oxidation of Tb^{3+} was attempted for both the cross and the radial flow cell.

For all attempts of Tb^{3+} oxidation in the flow cell no color change was observed. The absorbance spectra were measured using a cuvette of 10 mm path length instead of 0.1 mm to detect lower concentrations of Tb^{4+}. Also for shorter path length, the absorbance spectra didn't show any sign of formed Tb^{4+} in solution. The formation of oxygen gas was observed while running the experiment. In the measured current response, the formation of too much oxygen in the cell translated in a sudden current drop, which is seen around 400 s and 600 s

for the electrolysis at 9 s and 18 s residence time respectively. When the current drop occurred the electrolysis was stopped immediately to prevent any damage done to the working electrode. In Figure 37 the measured current response in the flow cell is compared with the measured current response for Tb^{3+} oxidation in bulk electrolysis. From the comparison is found that the current response for the bulk electrolysis oxidation is more than double the current response in electrolysis in the flow cell. This might be due to the absence or a reduced amount of Tb^{3+} oxidation.

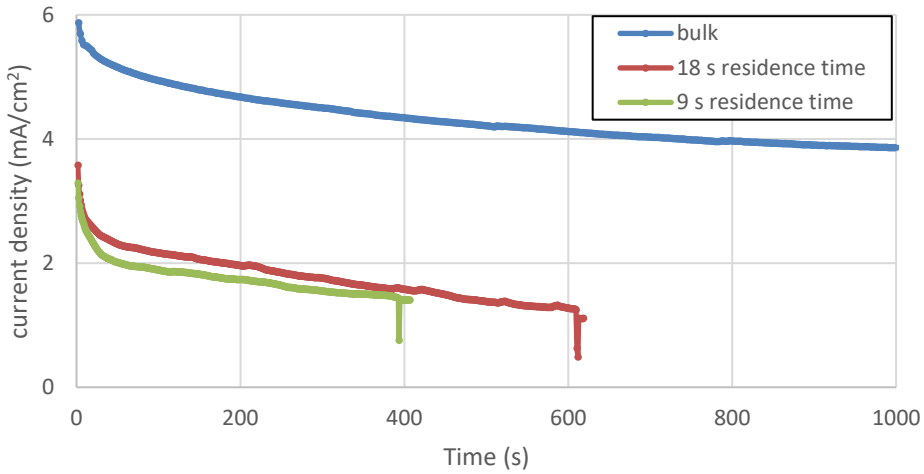

Figure 37: Current response measured for Tb^{3+} oxidation in bulk cell electrolysis and in flow cell electrolysis for 9 s residence time and 18 s residence time. Both electrolysis runs in the flow cell were stopped because of a sudden current drop due to excessive gas formation.

Furthermore, the measured current responses of flow cell electrolysis for various Tb-concentrations were compared. If Tb^{3+} gets oxidized in the flow cell, the measured current responses should increase upon increasing Tb concentration in solution.

In figure 38. The average measured current responses of two repetitions after 150 seconds of electrolyzing are displayed for Tb concentrations ranging from 40 mM up to 100 mM, the residence time of this oxidations were 9 seconds. A similar current response was observed for the concentrations between 40 mM and 70 mM, although for the higher concentrations an increasing trend was seen. From these results no conclusions were drawn, since the concentrations of 40 mM up to 70 mM indicate no Tb^{3+} was oxidized, Although the larger concentrations do seem to give an indication of Tb^{3+} oxidation.

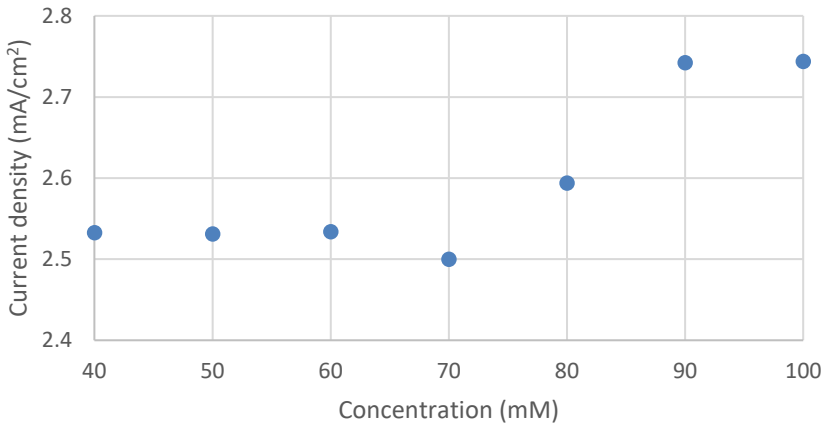

Figure 38: Current responses after 150 seconds of electrolyzing Tb^{3+} solutions of different concentrations: 40 mM, 50 mM, 60 mM, 70 mM, 80 mM, 90 mM and 100 mM Tb. The experiment was performed in the cross flow cell at a residence time of 9 seconds.

For the cross flow cell there is the possibility of using 2 working electrodes simultaneously. For the following experiment a working electrode block containing a Pt and a GC working electrode was used (Figure 39). The detection of possibly formed Tb^{4+} was attempted by instantaneous reduction at the second working electrode (GC), which is in series with the first working electrode. The Pt electrode will be referred to as working electrode 1 and the GC electrode as working electrode 2.

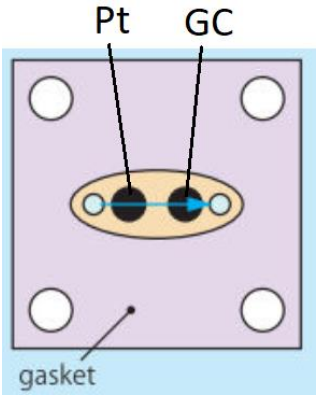

Figure 39: Working electrode block of the cross flow cell containing a Pt and a GC working electrode which can be controlled separately.

The current response of interest was measured at working electrode 2. According to the results of the part on Tb^{4+} reduction, Tb^{4+} reduction occurs for potentials below -0.3 V vs. Ag/AgCl in 3 M KCl. The potential for working electrode 1 was kept at +1.3 V vs. Ag/AgCl, while the potential at working electrode 2 was decreased between various experiments, starting from -0.1 V down to -0.5 V vs. Ag/AgCl in 3 M KCl.

The resulting current responses measured at working electrode 2 for different applied potentials are shown in Figure 40, the residence time was 9 seconds. The results correspond to what was observed in the chapter on Tb^{4+} reduction in bulk, for potentials of -0.3 V vs. Ag/AgCl and lower, Tb^{4+} reduction was indicated by a measured current response. At -0.3 V vs. Ag/AgCl the measured current value is much lower compared to the measured current at lower potentials, this corresponds to the faster reduction rates determined in the chapter on Tb^{4+} reduction in bulk.

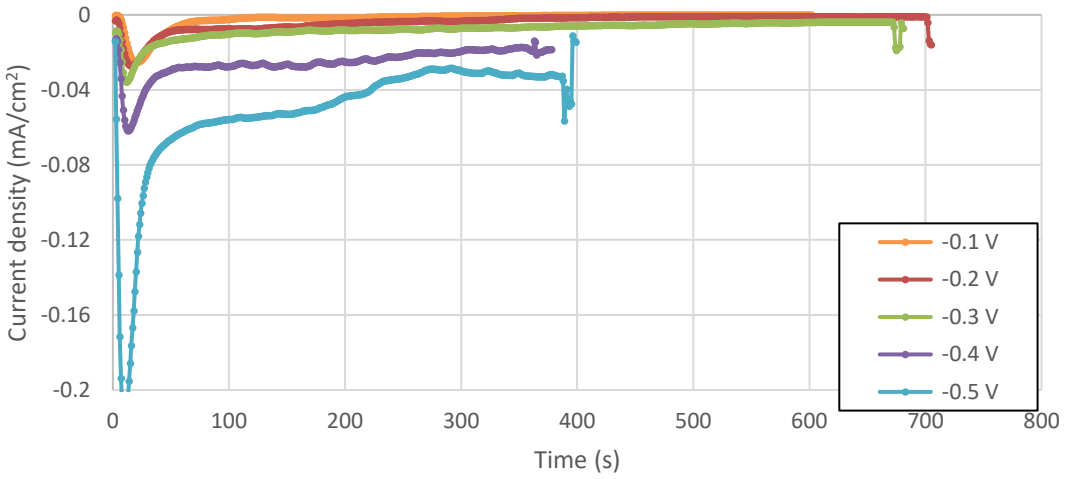

Figure 40: Measured current responses at the GC working electrode 2 for applying different potentials on working electrode 2: -0.1 V, -0.2 V, -0.3 V, -0.4 V and -0.5 V.

From this experiment can be concluded there was Tb^{4+} formed at the Pt working electrode, however based on the UV/VIS absorbance of the purged out solutions it should be a very small amount which was only detectable by the reduction at the second working electrode. Since there was no indication of Tb^{4+} in UV/VIS spectroscopy, it is expected the reduction also occurs spontaneously when no second GC working electrode is used in the system.

3.2. Divided cell

When oxidizing Tb^{3+} in bulk electrolysis, the working and counter electrode were both submerged in the bulk solution without any separation in between. To determine the influence of the possible back reduction of Tb^{4+} at the counter electrode, the counter electrode was separated from the bulk solution by a semipermeable membrane. Two different types of separating membranes were investigated, a CoralPor® frit and a porous glass frit, both were described in more detail in the experimental part. Before attempting oxidation of Tb^{3+} in the divided cell, impedance measurements were ran to determine the resistance resulting from the separation of the electrodes. In the electronic impedance spectroscopy the impedance is

measured over a range of frequencies. At 20 kHz the impedance value was extracted from the data, because at this point the impedance resulted exclusively from the separating membrane.

The obtained resistance values for the porous glass frit 22.5 Ω, the CoralPor® 380.8 Ω and no separating membrane 0.6 Ω are indicated in Figure 41. Before using both separating membranes, they were saturated with the solution by submerging them for at least 1 day prior to the experiments. The CoralPor® had a much higher resistance value compared to the porous glass frit.

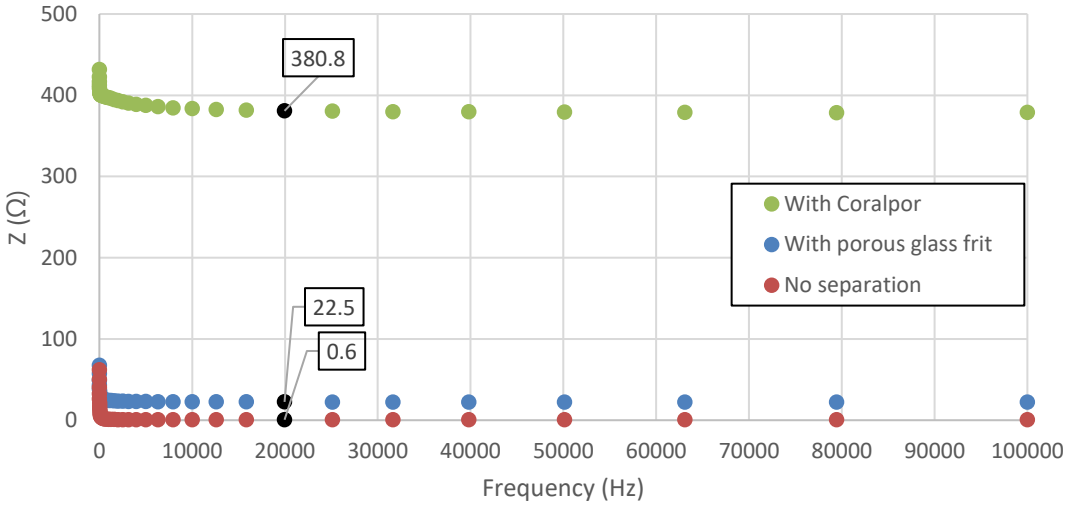

Figure 41: EIS spectra obtained from the divided cell using the CoralPor frit and porous glass frit and undivided cell. The resistance values are indicated at 19.953 kHz, because at this frequency the resistance is due to the used membrane.

3.2.1. Porous glass frit

Based on the resistance values above, Tb^{3+} oxidation was expected to be possible with the counter electrode separated from the bulk solution by a porous glass frit. When the electrolysis was started, the applied potential started to decrease. At the initial 10 to 15 seconds of electrolysis the potential was still in a region where oxidation of Tb^{3+} occurred, this resulted in an initial color change of solution near the working electrode similar as observed for electrolysis without a separating membrane. The color dissipated in the solution when the potential decreased further.

The ratio of surface area of working electrode to counter electrode was decreased by changing the size of working and counter electrodes. This way, the possible limitation of current flow caused by a too small counter electrode was prevented. However this didn't solve the potential drop observed in Figure 42, so the problem isn't caused by a too small counter electrode surface area. From the oxidation attempts with the porous glass frit no successful Tb^{4+} formation was obtained.

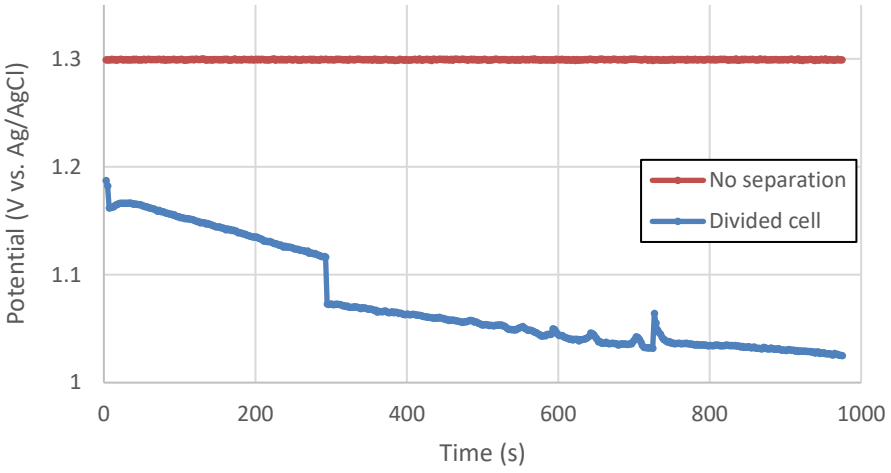

Figure 42: Applied potential for electrolysis in a cell without separating membrane and with porous glass frit.

3.2.2. CoralPor® frit

The CoralPor® frit usually finds its use in the semipermeable membrane for reference electrodes where it serves as a barrier between the KCl-solution and the solution in the electrolytic cell. Nevertheless the Tb^{3+} oxidation is attempted with a CoralPor® frit as separating membrane for the counter electrode chamber.

The same problem as for the porous glass frit occurred when attempting Tb^{3+} oxidation with the CoralPor® separating membrane, the potentiostat was unable to apply +1.3 V vs. Ag/AgCl in 3 M KCl. In Figure 43 the applied potential is shown. Also for the CoralPor® membrane different sizes of electrodes were tried with no success.

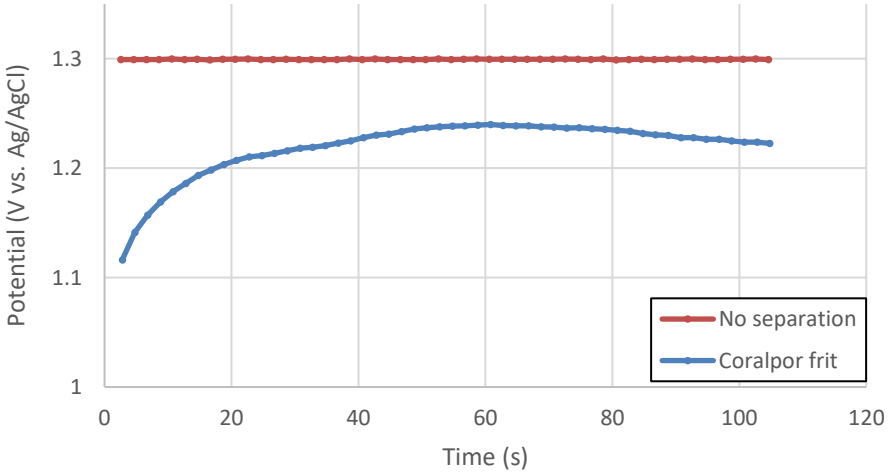

Figure 43: Applied potential for electrolysis in a cell without separating membrane and with CoralPor® frit.

3.2.3. Observed challenges and outlook

An observation made for both membranes is the formation of precipitate in the counter electrode chamber. Since no Tb-salt was present inside the separating chamber, the formed precipitate was supposed to be K_2CO_3 as it was the only salt present next to the low concentration of 75 mM KOH. For the porous glass frit the precipitation inside the chamber was the only observation made, which could have anything to do with the problem of applying +1.3 V vs. Ag/AgCl in 3 M KCl. Since the applied potential difference from +1.3 V vs. Ag/AgCl was not proportional to the resistance measured for the different membranes, it was expected the problem was not solely from the increased resistance. A possible explanation might be precipitate formation in the small ion-transport channels of the semi-permeable membranes. However if this would be the only problem an initial applied potential of +1.3 V vs. Ag/AgCl in 3 M KCl would be expected to be possible.

A possible explanation for the malfunctioning with the CoralPor® might be the amount of current passing the membrane for electrolytic applications is in a larger order of magnitude compared to the amount of current passed in reference electrode applications. The CoralPor® frits used in electrolysis became white during the experiments. In figure 44 three CoralPor® frits are displayed: one unused, one used as a reference electrode and one used in a divided cell experiment. The frit used in reference electrode applications was used for several months, the slight coloration on the edges didn't harm the functionality of the frit. The frit used in the divided cell clearly changed from a clear, colorless frit to a white frit where the edges were corroded.

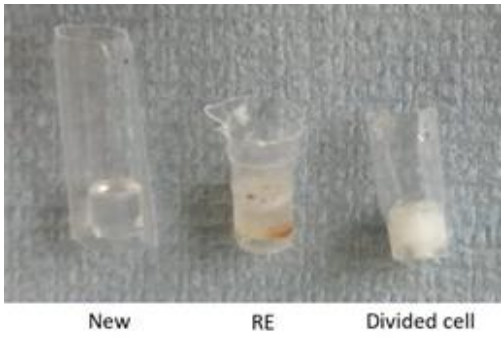

Figure 44: Three CoralPor® frits: a new frit which has not yet been used for any application, one that has been used as a separation membrane for a reference electrode and another one which has been used only once for Tb^{3+} oxidation.

The highly alkaline solutions were harmful to the CoralPor® membrane. Therefore, a frit was stored in 1 M KCl solution, a similar solution as they are stored in when used in a reference electrode. When electrolysis was attempted with the CoralPor® stored in 1 M KCl it was rinsed

with water and used in the same way as the other frits. Yet the same problem still occurred for the frit saturated with KCl solution as for the frits saturated in the highly alkaline K_2CO_3 solution.

Both separating membranes were found to be unstable in the highly alkaline solution of the investigated Tb^{3+} oxidation. Due to time limitation it wasn't possible to investigate the use of different membranes. A suggestion of another membrane to test in future research would be a Nafion™ membrane, as they are much thinner compared to the 2 tested membranes, if the precipitate formation in the channels would be the case this might be a possible solution to decrease the length the ion-transport inside the membrane. In addition to that, the increase of the surface area of the membranes might facilitate the ion transport. To minimize the precipitation in the counter electrode chamber the volume of the counter electrode chamber could be increased, this way the influence of gas formation will be less significant on the concentrations in the separate compartment. All these suggestions could be implemented using a cell similar to the one sketched in figure 45 with the working electrode in the compartment at the right and the counter electrode in the compartment on the left.

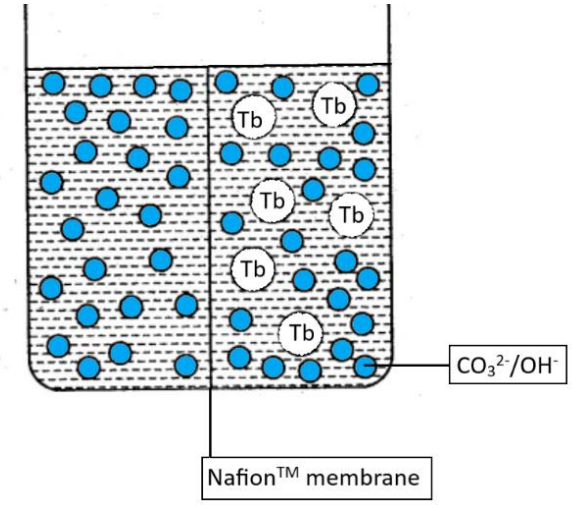

Figure 45: Sketch of suggested divided cell.

VI. Conclusions and outlook

In this work, the electrochemical oxidation of Tb^{3+} in aqueous carbonate solutions was investigated. In the following section the conclusions of all performed experiments were summarized. Since the time of research was limited and unforeseen, extrascientific challenges came along, not all experiments were able to be performed as thoroughly as hoped. Therefore suggestions were made for future researchers to go further into the discussed results.

From the CV-experiments regarding the Tb^{4+} reduction it was found that the reduction of Tb^{4+} occurred when using a GC working electrode around the potential of -0.3 V vs. Ag/AgCl in 3 M KCl. The Tb^{4+} reduction was not observed to take place when using a Pt working electrode, although there were reduction peaks observed in the CV scan of undetermined species. When Tb^{4+} reduction was converted to the bulk electrolysis using a RVC working electrode, it was found the complete Tb^{4+} reduction was possible for potentials of -0.3 V and lower vs. Ag/AgCl in 3 M KCl. The results from bulk electrolysis reduction confirmed the observed reduction peak in the CV scan was caused by Tb^{4+} reduction at the GC working electrode. When attempting to quantify the amount of Tb^{4+} in solution by integrating the measured current response over time for the Tb^{4+} reduction in bulk, it was observed the concentration determined electrochemically was very similar compared to the concentration determined with the estimated molar absorptivity[17,27]. Suggestions for future research were given to accurately determine the exact molar absorptivity of Tb^{4+} complex in aqueous carbonate solution. To start off a similar electrochemical reduction in bulk should be repeated to investigate why the measured current response didn't approach to zero in the performed experiment of this work. The electrochemical Tb^{4+} reduction with the purpose of quantifying Tb^{4+} in solution should be performed with an RVC electrode with a more accurately determined surface area. By measuring the absorbance values of different Tb^{4+} solutions and subsequently electrochemically reducing them, an accurate estimation of the molar absorptivity could be determined using the Lambert-Beer equation.

For the determination of the most efficient concentrations for K_2CO_3 and $TbCl_3{\cdot}6H_2O$ electrochemical oxidations of 2 hours were ran. It was found that 4 M K_2CO_3 was overall the most efficient when compared to 3 M and 5 M K_2CO_3. The 3 M K_2CO_3 was less efficient because there is a need for sufficient carbonate anions to form stable Tb^{4+}/carbonate complex. Although the 5 M K_2CO_3 solutions were less efficient compared to the 4 M K_2CO_3 solutions, the proposed reason for this was the carbonate-Tb^{3+} complex would be too strong for the hydroxide ions to coordinate with the formed Tb^{4+}. The coordination of the complex is both complicated and still unknown, however Varlashkin *et al*. reported the stable Tb^{4+} complex probably consists of both carbonate and hydroxide anions.[17] A too large concentration of

carbonate anions might cause a too strong complexation with carbonate anions, preventing the Tb^{4+} to partially coordinate with hydroxide anions. The Tb concentrations were varied between 40 mM and 100 mM. For the 2 hour electrolysis in 4 M K_2CO_3 the 70 mM Tb concentration was found to be the most efficient.

The influence of pH on the electrolysis was investigated. It was reported by Hobart *et al*. the pH has to be adjusted to 14 before oxidizing Tb^{3+}.[27] The electrolysis was ran for solutions at pH 13.1; 13.5 and 14. When the KOH concentration was increased too much, an insoluble precipitate formed. From these experiments was found no stabilization of Tb^{4+} occurred for solutions below pH 14.

The influence of the solutions' temperature on the electrochemical oxidation of Tb^{3+} was investigated. From these experiments it was found the stabilization of Tb^{4+} was most efficient at 5°C and found a decreasing efficiency for increasing temperatures. This result corresponds to the temperature experiments performed by Xiaojing *et al*. in tetrametaphosphate solutions, however the reasoning given by Xiaojing *et al*. does not hold for the electrochemical oxidation in aqueous carbonate solutions.[29] The Tb^{4+} complex in tetrametaphosphate solution was found to be very unstable over time, which was not the case for Tb^{4+} complex in aqueous carbonate solution. Another observation made from the temperature dependency experiments was the increased standard error for higher temperatures, indicating more consistent results for lower temperatures, increasing the reproducibility of the electrochemical oxidation.

The electrochemical oxidation of Tb^{3+} in aqueous carbonate solutions was examined in the flow cell. The working electrode surface versus volume of solution ratio is increased compared to bulk electrolysis, in combination with the mass transport being supported by the flow. For the CV experiments it was found that for residence times longer than 1 s the influence of flow on the CV of dilute sulfuric acid using a Pt working electrode was minimal. However for the Tb^{3+} oxidation attempts no indication of Tb^{4+} ions was observed in the UV/VIS absorbance spectra of the solutions purged out of the flow cell. When a second GC working electrode was used in the cell, indications were seen of Tb^{4+} reduction at the GC working electrode for potentials of -0.3 V and below vs. Ag/AgCl in 3 M KCl. This result confirms the Tb^{4+} reduction from the first chapter. However the flow cell oxidation did not show any advantage over the bulk electrolysis cell, expected to be due to the back reduction. For redox systems which occur without gas formation the flow cell is expected to be a very good candidate to improve the efficiency of the electrochemical oxidation, but due to the gas formation and possibly back reduction of Tb^{4+} the flow cell was no advantage for the system researched in this work.

For the electrochemical oxidation of Tb^{3+} in the divided cell the possible back reduction of the produced Tb^{4+} was prevented using a CoralPor® frit and a porous glass frit. For both separating membranes a precipitation was formed in the counter electrode chamber, which was supposed to be K_2CO_3. The precipitation probably caused the applied potential to drop, leading to inhibition of Tb^{3+} oxidation. The CoralPor® frit was already observed to be deteriorated after one electrolysis, indicating the conditions were too extreme for this membrane. As a suggestion for future research, membranes which are more commonly used in highly alkaline solutions could be tested. The precipitation might be inhibited by increasing the volume of the counter electrode chamber and using a thinner membrane with a larger surface area as sketched in Figure 45.

References

1. Radiation Therapy Benefits & Effectiveness - Targeting Cancer. https://www.targetingcancer.com.au/about-radiation-oncology/benefits-and-effectiveness/ (accessed 2020-11-26).

2. Nayak, D. & Lahiri, S. Application of radioisotopes in the field of nuclear medicine: I. Lanthanide series elements. *J. Radioanal. Nucl. Chem.* **242**, 423–432 (1999).

3. Cutler, C. S., Hennkens, H. M., Sisay, N., Huclier-Markai, S. & Jurisson, S. S. Radiometals for combined imaging and therapy. *Chem. Rev.* **113**, 858–883 (2013).

4. SPECT vs PET, https://radiopaedia.org/articles/spect-vs-pet (accessed 2020-11-28).

5. Cutler, C. S. *et al.* Current and potential therapeutic uses of lanthanide radioisotopes. *Cancer Biother. Radiopharm.* **15**, 531–545 (2000).

6. Lehenberger, S. M. Evaluation and application of the low energy electron emitter ^{161}Tb. (2010).

7. Müller, C., Van Der Meulen, N. P., Benešová, M. & Schibli, R. Therapeutic radiometals beyond ^{177}Lu and ^{90}Y: Production and application of promising α-particle, β^--particle, and auger electron emitters. *J. Nucl. Med.* **58**, 91S-96S (2017).

8. Van de Voorde, M., Van Hecke, K., Cardinaels, T. & Binnemans, K. Radiochemical processing of nuclear-reactor-produced radiolanthanides for medical applications. *Coord. Chem. Rev.* **382**, 103–125 (2019).

9. Poty, S., Francesconi, L. C., McDevitt, M. R., Morris, M. J. & Lewis, J. S. α-emitters for radiotherapy: From basic radiochemistry to clinical studies-part 1. *J. Nucl. Med.* **59**, 878–884 (2018).

10. Grünberg, J. *et al.* Anti-L1CAM radioimmunotherapy is more effective with the radiolanthanide terbium-161 compared to lutetium-177 in an ovarian cancer model. *Eur. J. Nucl. Med. Mol. Imaging* **41**, 1907–1915 (2014).

11. Kassis, A. I. *et al.* Radiotoxicity of ^{125}I in mammalian cells. *Radiat. Res.* **111**, 305–318 (1987).

12. Pomplun, E. & Sutmann, G. Is Coulomb explosion a damaging mechanism for ^{125}IUdR? in *Int. J. Rad. Biol.* **80**, 855–860 (2004).

13. Pomplun, E. Auger electron spectra: The basic data for understanding the Auger effect. in *Acta Onc.* **39**, 673–679 (2000).

14. IAEA Research Reactor Database, https://nucleus.iaea.org/RRDB (accessed 2020-12-04).

15. Nudat 2. https://www.nndc.bnl.gov/nudat2/ (accessed 2020-12-04).

16. Cotton, S. *Lanthanide and Actinide Chemistry*. *Lanthanide and Actinide Chemistry* (2006). doi:10.1002/0470010088.

17. Varlashkin, P. G., Begun, G. M. & Peterson, J. R. On the nature of tetravalent terbium in carbonate-hydroxide solutions. *J. Less-Common Met.* **109**, 123–134 (1985).

18. Propst, R. C., Nemours, E. I. P. De & Carolina, S. Electrochemical Oxidation of Terbium (3) At the Conducting Glass Electrode. **36**, 1085–1094 (1974).

19. Horwitz, E. P., Delphin, W. H., Bloomquist, C. A. A. & Vandegrift, G. F. Radiochemical and isotope separations by high-efficiency liquid-liquid chromatography. *J. Chromatogr. A* **125**, 203–218 (1976).

20. Monroy-Guzman, F.; Salinas, E. J. Separation of Micro-Macrocomponent Systems : ^{149}Pm – Nd , ^{161}Tb-Gd , ^{166}Ho-Dy and ^{177}Lu-Yb by Extraction Chromatography. *J. Mex. Chem. Soc.* **59**, 143–150 (2015).

21. Lahiri, S., Volkers, K. J. & Wierczinski, B. Production of ^{166}Ho through ^{164}Dy(n,γ) ^{165}Dy(n, γ)^{166}Dy(β-)^{166}Ho and separation of ^{166}Ho. *Appl. Radiat. Isot.* **61**, 1157–1161 (2004).

22. Tolmachev, V., Bernhardt, P., Forssell-Aronsson, E. & Lundqvist, H. ^{114m}In, a candidate for radionuclide therapy: Low-energy cyclotron production and labeling of DTPA-D-Phe-octreotide. *Nucl. Med. Biol.* **27**, 183–188 (2000).

23. Qiang, S., Zhijian, W. & Chongli, G. Solvent extraction of terbium(III, IV) periodate complexes with quaternary amine. *Solvent Extr. Ion Exch.* **13**, 275–288 (1995).

24. Su, Q. Wu, Z. Gao, C. Solvent extraction of tetravalent terbium Tb(IV) and other trivalent rare earths with quaternary amine. *Int. solvent Extr. Conf.* **1**, 605–610 (1996).

25. Ghiorso, A., Harvey, B. G., Choppin, G. R., Thompson, S. G. & Seaborg, G. T. New element mendelevium, atomic number 101 [8]. *Phys. Rev.* **98**, 1518–1519 (1955).

26. Campbell, D. O. Rapid rare earth separation by pressurized ion exchange chromatography. *J. Inorg. Nucl. Chem.* **35**, 3911–3919 (1973).

27. Edward Hobart, D. & Studies, S. Electrochemical and Spectroscopic Studies of Some Less Stable Oxidation States of Selected Lanthanide and Actinide Elements. (1981).

28. Vanýsek, P. *CRC Handbook of Chemistry and Physics, 92th Edition*. *J. Phys. Chem. Ref. Data* **18**, (1978).

29. Li, X., Dong, W., Qi, Y., Wang, D. & Yang, R. Studies on the stabilization of terbium(IV) in aqueous tetrametaphosphate solution. *Polyhed.* **10**, 1479–1483 (1991).

30. Payne, G. F. & Peterson, J. R. Oxidation studies of selected lanthanides in acetonitrile. *J. Less-Common Met.* **126**, 371–377 (1986).

31. Volkert, W. A. & Huffman, T. J. Therapeutic radiopharmaceuticals. *Chem. Rev.* **99**, 2269–2292 (1999).

32. Liu, S. & Edwards, D. S. Bifunctional Chelators for Therapeutic Lanthanide Radiopharmaceuticals. *Bioconjug. Chem.* **12**, 653–653 (2001).

33. Heppeler, A., Froidevaux, S., Eberle, A. & Maecke, H. Receptor Targeting for Tumor Localisation and Therapy with Radiopeptides. *Curr. Med. Chem.* **7**, 971–994 (2012).

34. Elgrishi, N. *et al.* A Practical Beginner's Guide to Cyclic Voltammetry. *J. Chem. Educ.* **95**, 197–206 (2018).

35. Flowcell. https://www.als-japan.com/ (accessed 2021-04-08)

AFDELING MOLECULAIR DESIGN EN SYNTHESE
Celestijnenlaan 200F bus 2404
3001 LEUVEN, BELGIË
tel. + 32 16 32 04 76
thomas.cardinaels@sckcen.be
www.sckcen.be